Structural and thermochronological constraints on the movement history of the Montosa fault, New Mexico

Rose-Anna Behr[1], Laurel B. Goodwin[2], and Shari A. Kelley
Department of Earth and Environmental Science, New Mexico Institute of Mining and Technology, Socorro, NM 87801
[1]Now at: Nixon Park, 5922 Nixon Drive, York, PA 17403;
[2]Now at: Department of Geology and Geophysics, University of Wisconsin-Madison, 1215 W. Dayton St., Madison, WI 53706

Abstract

The movement history of brittle faults in New Mexico has generally been difficult to constrain for two primary reasons. First, a scarcity of piercing points precludes the calculation of total slip vectors, and second the faults have typically been reactivated and therefore record different parts of the region's complex tectonic history. Yet a number of critical tectonic questions, such as the importance of strike-slip displacement east of the Colorado Plateau during the Laramide orogeny, require a better understanding of the evolution of these brittle fault systems. Consistent patterns of minor faulting and folding associated with faults of known slip history (e.g., the San Andreas fault) suggest that such patterns can be used to interpret the movement history of poorly understood faults. We used this approach in conjunction with apatite fission-track analysis to unravel the history of the Montosa fault of central New Mexico. This 90-km-long, north-northeast-striking, west-dipping fault shows reverse separation over much of its length. The youngest rocks cut by the fault are Late Permian in age, indicating that the fault is younger than Late Permian. The southernmost part of the fault exhibits normal separation and structures that indicate that it was reactivated as a normal fault during Rio Grande rift extension. Fission-track data indicate that significant dip-slip displacement across the fault ceased before 14–25 Ma, when both footwall and hanging wall were exhumed and cooled together.

Minor faults and folds have been grouped by strain (shared patterns of shortening and extension directions). These groups, and crosscutting relationships observed by previous workers, suggest that the Montosa fault was active as a dextral-reverse oblique, a dextral, and a sinistral fault before accommodating extension during rifting. We interpret the dextral-reverse and dextral faulting as Laramide in age and suggest that sinistral faulting occurred during the tectonic transition between the Laramide orogeny and Rio Grande rift extension.

Introduction

The Laramide orogeny has fascinated researchers for years because deformation occurred so far inland—as much as 2,000 km from the ancient continental margin (e.g., Rodgers 1987). Differing explanations of this intracontinental deformation have been proposed. The most widely accepted popular hypothesis is that shallowing of the eastward-subducting Farallon plate caused both deformation and arc volcanism to sweep inland (Snyder et al. 1976; Coney and Reynolds 1977; Dickinson and Snyder 1978; Keith 1978). Alternatively, it has been suggested that the Laramide orogeny was produced by the collision and subsequent northward translation (dextral oblique convergence) of a foreign terrane with the western margin of North America (Maxson and Tikoff 1996). Regardless of the driving force, the Colorado Plateau apparently behaved as a relatively rigid block that transferred deformation eastward into New Mexico (e.g., Hamilton 1981; Chapin and Cather 1981). The magnitude and direction of translation and rotation of the plateau is disputed, though it is evident that faults and folds north and east of the plateau must record this movement. Karlstrom and Daniel (1993) estimated 100–170 km of displacement on north-striking faults in New Mexico based on the offset of piercing points in the Proterozoic basement and suggested that much of this movement was Laramide in age. Isopach and pinch-out trends in Mesozoic sedimentary rocks in northern New Mexico allow a minimum of 33–46 km of dextral offset along the eastern margin of the Colorado Plateau and as much as 110 km of right-lateral slip across the entire fault system east of the Colorado Plateau (Cather 1999). These interpretations suggest significant northward translation of the Colorado Plateau with respect to the region to the east. Woodward et al. (1997), however, maintained that a maximum of 5–20 km of dextral strike-slip displacement occurred across New Mexico, from which they inferred that the plateau was translated eastward and the faults were largely reverse. Woodward (2000), Lucas et al. (2000), and Ingersoll (2000) also argued for relatively small (< 20 km) amounts of dextral displacement during Laramide-age deformation.

Laramide activity has been demonstrated on a number of faults in New Mexico, but the variation in interpretations of the kinematics of these faults illustrates the difficulty of resolving this controversy. Among the largest of these structures are the Nacimiento fault, the Rio Puerco fault zone, the Picuris–Pecos fault, the Tijeras–Cañoncito fault zone, and the Montosa fault (Fig. 1). The north-striking Nacimiento fault has been interpreted as both a dextral reverse oblique-slip fault (Baltz 1967; Stewart and Hibbard 1992; Pollock et al. 2004 this volume) and a reverse fault (Woodward 1976). The Rio Puerco fault zone was reported to have dextral oblique-slip offset (Slack and Campbell 1976). The north-striking Picuris–Pecos fault was originally interpreted as a reverse, Laramide-age fault, but a dextral strike-slip component was later noted, and the fault was interpreted as being Proterozoic in age (Miller et al. 1963). More recently Bauer and Ralser (1995) suggested that this fault was part of a positive flower structure, in which deformation was partitioned between a dominantly dextral strike-slip Picuris–Pecos fault and a series of parallel, dominantly reverse faults. They noted evidence for both Proterozoic and Laramide-age movement. Previous workers have interpreted Laramide-age deformation on the northeast-striking Tijeras–Cañoncito fault zone as dextral reverse oblique (Ferguson et al. 1999), and right-lateral strike-slip, with a northwest-side-down component of movement (Kelley and Northrop 1975; Lisenbee et al. 1979; Chapin and Cather 1981; Abbott and Goodwin 1995; Abbott et al. 2004 this volume). Studies of the fault system generally recognize that the fault has had a complex history; for example, Abbott et al. (2004 this vol-

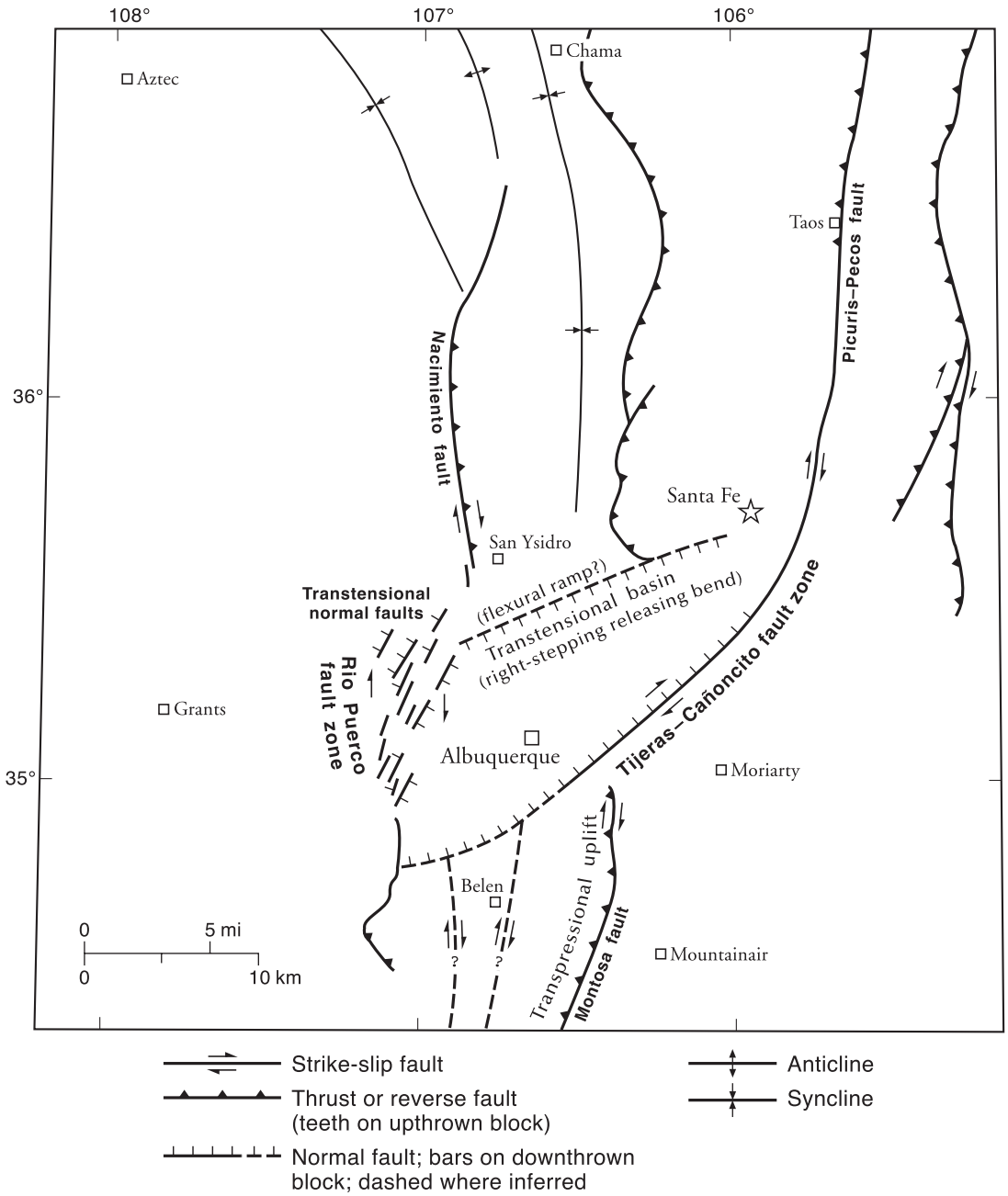

FIGURE 1—Laramide-age faults and folds in northern and central New Mexico. Map and kinematic interpretations from Cather (1992).

ume) present evidence that it initiated as a dextral strike-slip fault during the Laramide orogeny, and was reactivated as a sinistral transfer fault during Rio Grande rift extension.

Various orientations of maximum principal stress and strain have been inferred for the Laramide orogeny from fault displacements using piercing lines (e.g., Bauer and Ralser 1995; Woodward et al. 1997; Cather 1999), dike orientations (e.g., Rehrig and Heidrick 1976), kinematic indicators (e.g., Abbott 1995; Bauer and Ralser 1995), fault geometries (e.g., Cabezas 1987), and inversion of minor fault data (e.g., Erslev 2001). Several authors have proposed a multistage Laramide deformation history (e.g., Knepper and Maars 1971; Gries 1983; Cabezas 1991; Livaccari 1991; Erslev 2001), whereas others maintain that a single deformation event occurred (e.g., Reiches 1949; Stone 1969). Most authors have inferred east to northeast shortening during the Laramide orogeny, which, like the kinematic interpretations referred to above, does not resolve either the question of how deformation was transferred into New Mexico, or how it was accommodated.

The magnitude of dextral strike-slip motion across the north-northeast striking Montosa fault, like other faults in New Mexico, is disputed. Originally the fault was interpreted as a reverse fault (Stark and Dapples 1946; Reiche 1949; Stark 1956; Kelley 1977). More recently evidence for dextral oblique-slip movement has been found (Cabezas 1987; Hayden 1991). Cather (1992) hypothesized that the Tijeras–Cañoncito fault zone acted as a right step in a dextral shear system including the Picuris–Pecos fault to the north and the Montosa fault to the south (Fig. 1). Our work, which incorporates structural analysis of folds and minor faults as well as apatite fission-track thermochronology, indicates that the Montosa fault was most likely formed during the Laramide orogeny and was reactivated during the early

phases of Rio Grande rift extension before 25 Ma. We interpret minor structures as indicating that the fault accommodated both reverse and dextral strike-slip shearing at early stages in the fault history. It was reactivated as a sinistral strike-slip fault before accommodating normal movement during extension.

Previous work

The Montosa fault is a 90-km-long, north-northeast-striking fault that bounds the east side of the Manzano and Los Pinos Mountains of central New Mexico (Fig. 2). The fault strike varies from N40°W at the northern tip to due east in one of the three prominent fault bends. The fault dip varies from 55° to 75° west, approximately parallel to the foliation in the Proterozoic basement. The northern two-thirds of the fault show reverse separation with Proterozoic schist, quartzite, gneiss, and granitoid of the hanging wall juxtaposed against Pennsylvanian and Permian sandstone, mudstone, limestone, and conglomerate of the footwall (Stark and Dapple 1946; Reiches 1949; Stark 1956). An exception is a 1.2 km stretch in Sand Canyon north of Abo Pass, where Pennsylvanian limestone is exposed on both sides of the fault (Stark 1956). The southern third of the fault shows normal separation with Pennsylvanian and Permian rocks juxtaposed by the fault (Cabezas 1987). The fault has been interpreted as Laramide (Late Cretaceous–early Tertiary) in age because it cuts Permian sedimentary rocks (Stark and Dapples 1946; Hayden 1991).

A COCORP (Consortium for Continental Reflection Profiling) seismic line that followed US–60 (Fig. 2) across Abo Pass and into the Rio Grande rift revealed a strong reflector interpreted as the Montosa fault (de Voogd et al. 1986). This reflector dips steeply westward at the surface and shallows at depth. The Paloma fault, which lies west of the Montosa fault, and the Cenozoic Los Pinos normal fault, which bounds the west side of the Los Pinos Mountains, either sole into or are truncated by the Montosa fault at depth.

The Montosa fault is east of the Carthage–La Joya Basin, an Eocene (Laramide-age) basin filled with the synorogenic sediments of the Baca Formation (Cather and Johnson 1986). Paleocurrent trends and clast-size distribution measured in the Baca Formation point to a source area west of the preserved basin margin. This Laramide highland, called the Sierra uplift (Cather 1983), is now buried beneath the Rio Grande rift. The uplift associated with movement on the Montosa fault apparently did not contribute sediment to the Carthage–La Joya Basin. The basin was highly disrupted by rift-related faulting and most of the Baca Formation has been removed by erosion, suggesting significant post-Eocene denudation in the area east of Socorro.

The low-temperature (~ 60–120° C) cooling histories of the Los Pinos and Manzano Mountains were determined by Kelley et al. (1992) using apatite fission-track (AFT) thermochronology. The AFT data record Laramide-age deformation and Eocene erosion as well as cooling during early stages of extension associated with development of the Rio Grande rift. Higher elevations within the Manzano Mountains record late Eocene to early Oligocene denudation (from 47 ± 7 to 29 ± 3 Ma). Samples from lower elevations on the west side of the Manzano Mountains may reflect the early stages of Rio Grande rift formation, but the AFT ages have large margins of error due to low apatite yield and low uranium content. The apatite fission-track ages of an age-elevation transect in the Los Pinos Mountains range from 44 ± 7 to 60 ± 20 Ma, indicating cooling during Laramide denudation and subsequent Eocene erosion.

Principles and methods

We used both structural and thermochronologic data to evaluate the tectonic evolution of the Montosa fault. Minor faults, folds, and other structures were used to constrain the kinematic history of the fault and evaluate the possibility of strain partitioning between the fault and adjacent areas. AFT age and length data collected at equal elevations on either side of the Montosa fault in the Manzano and Los Pinos Mountains allowed us to constrain the timing of faulting with respect to cooling through 60–120° C. Stratigraphic relationships were used to further evaluate the timing of deformation.

Kinematic constraints from structural analysis

The Montosa fault is no longer active, and there are no piercing points to record the total slip vector. Thus, we must rely on stratigraphic separation and the distribution and character of minor structures that are spatially associated with the fault to constrain its movement history. In order to evaluate what can be learned from these minor faults and folds, we consider patterns of structures associated with the extensively studied San Andreas fault in the following paragraphs. The purpose of this exercise is to determine what can be learned from structural patterns in an active fault with known kinematic history, so that we can apply this approach to the Montosa fault zone.

In-situ stress measurements indicate that the current maximum horizontal stress is oriented at nearly right angles to the San Andreas fault over a large area in California (e.g., Mount and Suppe 1992; Zoback et al. 1987; Zoback and Healy 1992), although it is locally oriented 25–45° clockwise from strike adjacent to the fault (e.g., Castillo et al. 1997). Deformation in the vicinity of the San Andreas fault is strongly partitioned (see reviews by Teyssier et al. 1995; Tavarnelli 1998): right-lateral strike-slip movement is localized along the fault; in contrast, structures to the southwest and northeast record significant fault-perpendicular shortening. Minor fault and fold data collected both directly adjacent to the strike-slip San Andreas fault and subsidiary faults and from areas that are accommodating fault-perpendicular shortening are notable for several reasons (Chester and Logan 1987; Tavarnelli 1998; Ghisetti 2000): (1) minor faults parallel to the major faults are conspicuously absent; (2) minor faults exhibit a complete range of dip-slip, strike-slip, and oblique-slip kinematics; (3) maximum principal stress orientations inferred from the minor fault data are at a high angle to the main fault, similar to measured in-situ stresses; (4) the latter stress determinations are similar to those calculated from minor earthquake data in the same areas, indicating that ongoing deformation is similar to that recorded by minor structures. Although minor faults parallel to the San Andreas fault are rare, minor fault and fold patterns within a kilometer of the primary strands of the San Andreas fault system are distinctly different from those farther from the fault system. These differences, summarized below, suggest that the patterns of minor structures can be used both to constrain movement on associated large-scale faults and to evaluate deformation partitioning.

Minor fault data collected in the Salinian block, west of the San Andreas fault in central California (Tavarnelli 1998), are summarized in Figure 3A. Structures in this area include folds that trend subparallel to the fault and plunge shallowly to moderately northwest or (less commonly) southeast, and northwest-striking thrust faults that dip both southwest and northeast. The data shown in Figure 3A are typical of 127 faults studied (Tavernelli 1998); most of these data appear to have been collected more than 1 km from the major faults of the San Andreas system. They record shortening at nearly right angles to the San Andreas fault and

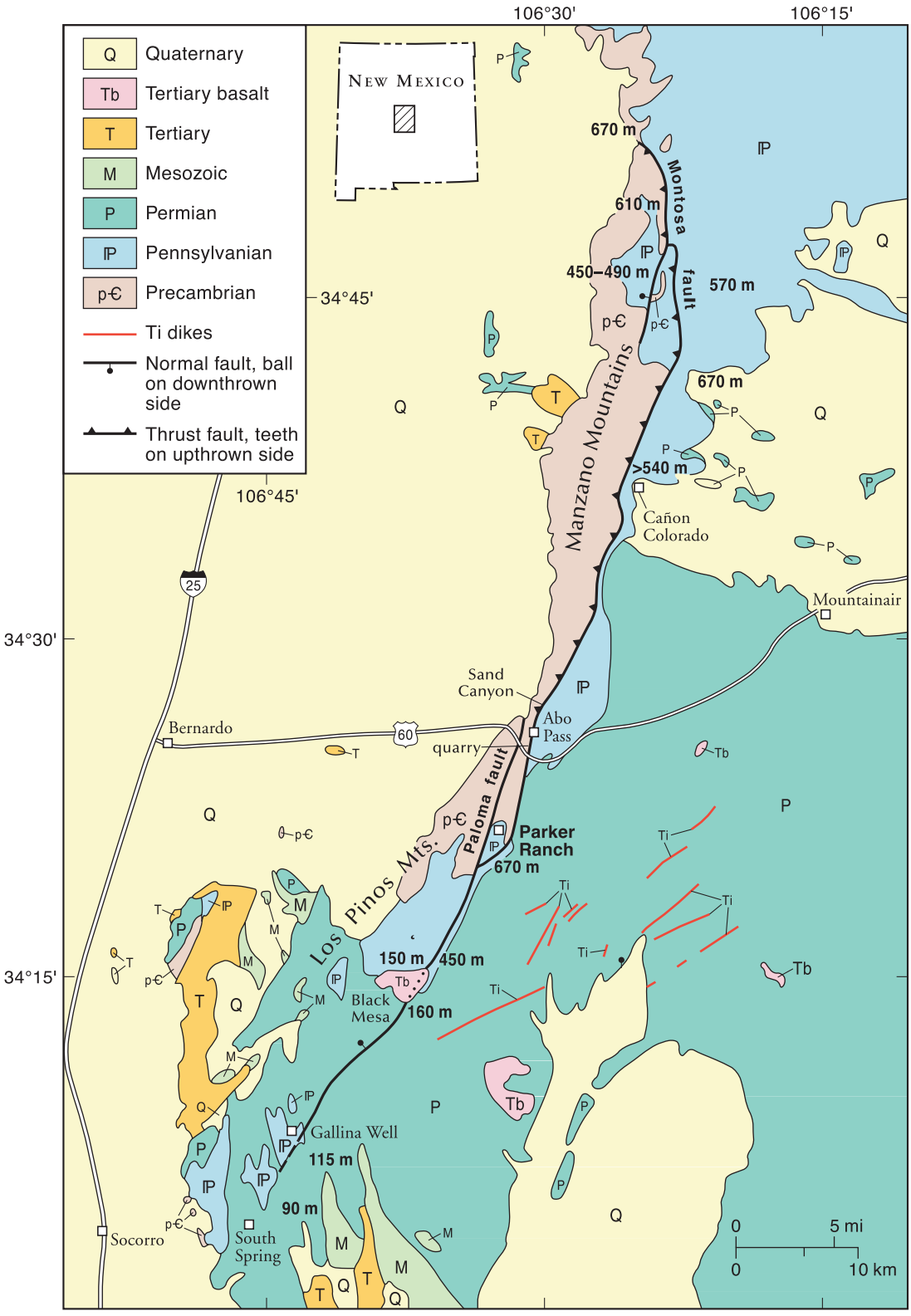

FIGURE 2—The west-dipping Montosa fault and surrounding area. Location of study area is shown in upper left corner. Numbers indicate vertical separation in meters across the fault. North of Black Mesa, separation is reverse (barbs point toward hanging wall), and south it is normal (ball and post symbols point toward hanging wall). Location of Sais Santa Fe Quarry shown as **quarry**. Base map modified from New Mexico Bureau of Geology (2003)
.

subvertical extension or crustal thickening. These structures therefore record nearly coaxial deformation.

Faults are typically surrounded by zones of damage, within which minor structures overprint regional structures. The width of a damage zone is determined by the density of fault-zone structures, which decreases with distance from a given fault; damage-zone width may vary depending on which structures are used to define it. For example, the width of the Punchbowl damage zone defined by the extent of fault-related microfractures is more than triple that defined by macroscopic shear fractures and minor faults (Wilson 1999).

Within the damage zone of the Punchbowl fault, a dormant strand of the San Andreas fault system in southern California that accommodated approximately 20 km of right-lateral strike-slip before exhumation (Chester and Logan 1987), structures have a very different character than those described by Tavernelli (1998; Fig. 3B). The Punchbowl fault is located in a bend in the San Andreas fault system, so it accommodated a component of reverse slip in addition to dextral shear. The fault dips steeply to the southwest, rather than vertically, and vertical separation records the reverse movement history. The Punchbowl damage zone defined by minor faults and shear fractures varies in width but extends roughly 30 m from the Punchbowl fault, and is dominated by dextral strike-slip faults (Fig. 3B; Chester and Logan 1987). The steeply plunging fault B-axis (the intermediate principal strain axis) was determined from fold and minor fault data, and the slip direction on the Punchbowl fault was inferred from that axis. Steeply plunging fold axes were determined from folded strata up to 1 km from the fault. In contrast to areas farther from the fault, such as the Salinian block, minor structures within a kilometer of the Punchbowl fault record noncoaxial deformation, with dextral shear accommodating shortening and a shallowly plunging maximum extension direction.

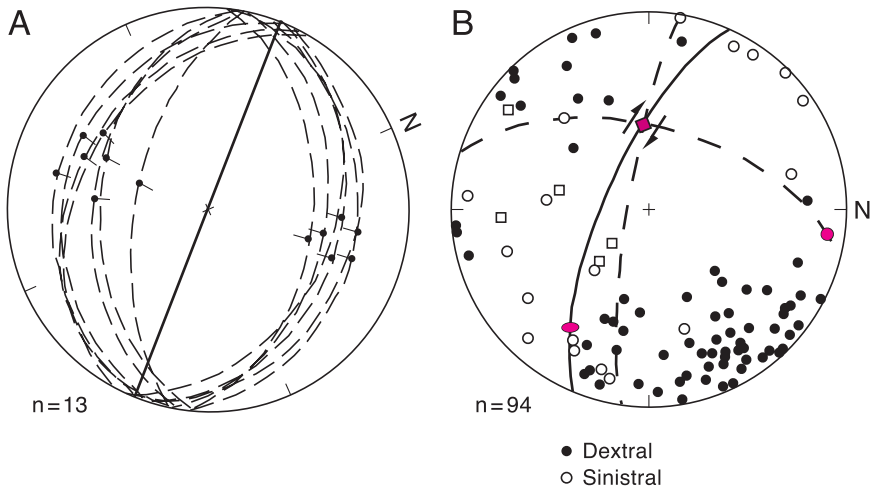

FIGURE 3—Lower hemisphere, equal area net plots of minor faults associated with the San Andreas fault system. The main fault trace is shown as a solid line in each case; figures have been rotated to facilitate comparison with data from the Montosa fault. (**A**) faults from Bodega Head, Salinian block, west of the San Andreas fault, showing representative orientations of thrust faults (dashed lines) and slickenside striae (solid circles with tails indicating slip directions). After Tavarnelli (1998). (**B**) Poles to minor faults within the damage zone of the Punchbowl fault; key indicates fault type. Dashed lines separate fields of dextral and sinistral strike-slip faults. Red square records the fault B-axis inferred from minor faults and folds. Red ellipse is the inferred slip direction; red circle is the inferred maximum principal stress orientation. See text for further explanation. Modified from Chester and Logan (1987).

As mentioned previously, the trend of the maximum principal stress inferred from structures both within and outside the damage zone of the San Andreas fault is close to perpendicular to the fault. Slip sense therefore cannot be inferred from the stress orientation alone. The maximum principal stress orientation probably reflects the mechanically weak nature of the fault zone, as suggested previously by a number of workers (e.g., Lachenbruch and Sass 1980; Mount and Suppe 1992; Zoback et al. 1987; Zoback and Healy 1992). However, the minor structures record the deformation history. The types and orientations of minor faults in the damage zone, vertical separation, and folds up to 1 km from the Punchbowl fault, together can be used to infer slip sense. The minor faults record noncoaxial, dominantly dextral shear within the damage zone, vertical separation records the reverse component of slip, and the fold axes and faults can be used to determine the fault B-axis and, therefore, the orientation of the slip vector. Strain calculations (e.g., Marrett and Allmendinger 1990) would indicate maximum shortening at a high angle to the fault but would also show a shallowly plunging major principal strain axis (maximum extension direction), reflecting the dominance of strike-slip over reverse motion on the fault.

Subsidiary structures farther from the fault zone also record shortening at a high angle to the fault. However, because deformation is partitioned, this shortening was accommodated by coaxial deformation. Conjugate thrust faults and folds result in a subvertical major principal strain axis, or direction of extension, recording crustal thickening. In the absence of deformation partitioning we would anticipate that structures located outside the damage zone of a given fault would record deformation similar to that adjacent to the fault. We apply these principles in our analysis of minor structures associated with the Montosa fault.

Fission-track analysis

The minimum age of faulting and the depth of currently exposed rocks during faulting can be constrained using apatite fission-track thermochronology, a well-established method for constraining the low-temperature thermal history of rocks (e.g., Naeser 1979; Gallagher et al. 1998). The principles behind fission-track analysis are discussed in detail elsewhere in this volume (see fig. 2, Kelley and Chapin 2004 this volume) and are only briefly mentioned here. Fission tracks are submicroscopic damage zones in crystals produced by the spontaneous fission of ^{238}U. Fission-track annealing in apatite is controlled primarily by temperature, the duration of heating or cooling, and the chemical composition of the apatite. Tracks in apatite with > 0.5 wt% Cl are more resistant to annealing than those from apatites with < 0.5 wt% Cl (Green et al. 1986; Carlson et al. 1999). In a relatively stable geological environment where present-day burial temperatures are at a maximum, AFT age and mean track length decrease systematically with increasing depth and temperature (Naeser 1979; Fitzgerald et al. 1995). At temperatures less than ~ 60° C, fission tracks are retained, and annealing is minimal. The AFT ages in basement rocks at shallow depths (< 2–3 km) reflect the cooling history of the basement before attainment of the present thermal conditions, and the mean track lengths are general-

ly 12–4 μm (Gleadow et al. 1986). At temperatures above ~ 60° C, rocks enter the temperature range known as the partial annealing zone (PAZ). With increasing temperature and depth through the PAZ, AFT ages are reduced, track lengths decrease (typically from approximately 13 μm to 8 μm), and the spread in the track-length distribution increases. Finally, at the base of the PAZ, tracks that form are quickly destroyed, and the fission-track age is effectively zero. The base of the PAZ is typically reached at temperatures between ~ 110° C and 140° C, depending on the apatite composition and the duration of heating. Combined AFT age and length data can be used to constrain the low-temperature cooling history of the host rock using annealing models calibrated with short-term laboratory annealing data and long-term geologic data (Laslett et al. 1987; Crowley et al. 1991; Carlson et al. 1999).

The Montosa fault

Three kilometers of the fault trace were mapped in detail (1:12,000) in Sand Canyon, through Abo Pass, and along the edge of the Sais Santa Fe Quarry (Fig. 2). Two kilometers at the southern end of the fault near Gallina Well were also mapped in detail. We focused on the damage zone of the fault, within which macroscopic fracture densities are higher than in surrounding areas. The majority of mapping and sample collection therefore took place within 0–1,000 m of the fault because the density of fractures and minor faults drops off dramatically farther from the fault. Exceptions are noted in the following sections. Detailed mapping helped resolve differences in previous workers' maps (Myers and McKay 1971, 1974; Myers 1977; Myers et al. 1981, 1986; Cabezas 1987). Reconnaissance mapping and measurements were compiled in the Manzano and Los Pinos Mountains. Because the Montosa fault itself is poorly exposed and shows no kinematic indicators, minor faults associated with the Montosa fault were examined in the field, in hand sample, and in thin section to constrain movement sense. Sense of slip on minor planes was determined by examining slickensides, slickenside striae, slickenfibers, and secondary fractures such as Riedel shears (Fig. 4; Fleuty 1975; Petit 1987). The sense of slip on minor faults of different orientations was used, in addition to the orientations of fold hinges and overall fault geometry, to evaluate strain in the vicinity of the fault.

Vertical separation was estimated by determining the difference in elevation of a given stratigraphic contact on either side of the fault. Where the fault has multiple strands, separation across the entire fault zone was estimated. If two like contacts were not exposed, vertical separation was extrapolated using stratigraphic thicknesses. For example, in the Manzano Mountains, the Proterozoic–Pennsylvanian contact is exposed west of the fault. East of the fault only contacts within Pennsylvanian strata are exposed. In this case the elevation of the Proterozoic–Pennsylvanian unconformity was estimated by subtracting the known stratigraphic thickness of the Pennsylvanian section (Myers and McKay 1971, 1972; Myers et al. 1986). This is a reasonable assumption because significant changes in thickness or angular unconformities in the Pennsylvanian–Permian section across the Montosa fault, which could be related to Ancestral Rockies deformation, have not been reported in this area (e.g., Myers 1982). In the Los Pinos Mountains, the Proterozoic–Pennsylvanian unconformity is exposed west of the fault, and Permian rocks are exposed on the east. South of Black Mesa, vertical separation can be determined from the difference in elevation of Permian contacts exposed on either side of the Montosa fault. Again, Pennsylvanian and Permian sedimentation was not noticeably influenced by the Montosa fault in this area during Ancestral Rockies deformation (Stark and Dapples 1946). No piercing points were found to constrain lateral displacement.

Main fault system

Stratigraphic separation along the fault varies from reverse at the northern tip to normal at the southern tip (Fig. 2). A maximum of 670 m of reverse separation is observed along the northern half of the fault. The minimum reverse separation of 150 m is recorded just north of Black Mesa. By comparing the maximum elevations of exposed stratigraphic contacts in the vertical limb of a "drag" fold in the footwall in this area with the elevations of the same (horizontal) contacts in the hanging wall, it can be deduced that at least 90 m of normal throw occurred subsequent to reverse motion. Reverse separation before normal faulting was therefore 240 m. One hundred and sixty meters of normal separation was determined across a zone of anastomosing fault strands south of Black Mesa. Normal separation decreases to 90 m 3 km from the southern fault tip.

The northern third of the fault is poorly exposed due to vegetative cover. The central 45 km of the fault, however, are marked by a prominent ridge of vertical to overturned limestone beds in the footwall. The southern 16 km of the fault occupy a broad valley between cuestas and mesas. Three-dimensional exposure of the fault zone is found only in the railway cut at Abo Pass, but the fault trace is easily followed.

Where exposed, the Montosa fault is characterized by a zone of brittle deformation rather than a single slip plane. The well-exposed, 600-m-wide cross section of the fault in the railway cut at Abo Pass includes a 7-m-wide core zone, oriented N25°E 60°W, consisting of cataclasite, breccia, and jumbled boulder-sized clasts. Hanging-wall Proterozoic quartzite is juxtaposed against Pennsylvanian limestone in the footwall. On the north side of the railroad tracks, the northwestern edge of the fault core includes an approximately 30-cm-wide zone of angular quartzite clasts in a matrix of limy mudstone. The center of the fault core contains boulder-sized clasts of limestone. The southeastern edge of the core zone consists of relatively weak limy mudstone to shale, which may have accommodated some fault slip. Outside the fault core, quartzite and limestone beds are nearly parallel to the fault zone and are cut by minor reverse and normal faults in the damage zone. On the southwest side of the railroad tracks, the zone of quartzite clasts in limy mudstone matrix is absent, and the northwest side of the fault core is marked by a well-indurated quartzite breccia. The railway cut is the only location where minor faults within the fault core could be measured.

At the southern end of Grey Ridge, north of Black Mesa, the Montosa fault core is a partially exposed, foliated limy mudstone. The footwall damage zone contains shallowly dipping beds of Permian and Pennsylvanian rocks folded to a near vertical orientation adjacent to the fault. The hanging wall is Pennsylvanian limestone covered by Quaternary deposits. The hanging-wall beds also dip steeply to the west in the damage zone, proximal to the fault. Stratigraphic offset records 150 m of reverse separation. The core zone contains multiple foliations and crinoids and bivalves that have been flattened within the main foliation. In one area, the main foliation is oriented N82°E 61°N, and a secondary foliation is oriented N33°E 84° SE. Dextral shear of the secondary foliation across the main foliation planes is evident. The slip direction must be 90° from the intersection between these foliation planes, suggesting that a reverse component of movement accompanied dextral shear. Nearby, however, the main foliation strikes N45°E and a secondary foliation strikes N65°E, suggesting a component of sinistral slip. These observations suggest that foliations of different ages are present, recording multiple episodes of deformation.

The Paloma fault is a major imbricate branch of the Montosa fault (Kelley 1977). It is about 38 km long, dips west, and is nearly parallel to the Montosa fault (Fig. 2). The northernmost junction of the Paloma and Montosa faults is located near Cañon Colorado; to the south, the faults join at the right step in the Montosa fault south of Parker Ranch. The Paloma fault juxtaposes Proterozoic rocks capped by Pennsylvanian sandstone and limestone and shows at least 180 m of reverse separation by Cerro Montoso, just southwest of Parker Ranch. Ten kilometers north of US–60, the Proterozoic Blue Springs Schist is structurally omitted by the fault, resulting in the juxtaposition of the Proterozoic White Ridge quartzite and the Proterozoic Sais Quartzite (Stark 1956). Stark (1956) therefore interpreted the Paloma fault as recording a minimum of 735 m of reverse separation, based on the minimum thickness of Blue Springs Schist.

Minor faults

Over 500 slickensides, slickenside striae, and slickenfibers were measured on small faults in the field (e.g., Fig. 4). Seven localities were examined for kinematic indicators. From north to south, these are Cañon Colorado, Sand Canyon, the Railway Cut, Sais Santa Fe Quarry, Parker Ranch, Gallina Well, and South Spring (Figs. 5, 6). With the exception of the South Spring area, kinematic indicators were evaluated within the damage zone, as defined in the field by the density of minor faults and shear fractures. As indicated in the following descriptions, the width of the damage zone varies along strike. In Cañon Colorado a few outcrops located 1.5 km east of the fault reveal good kinematic indicators in arkoses of the Permian Abo Formation. Slickenlines are common, and slickensides with a millimeter thick cataclasite layer are well developed. East of the Sand Canyon area, Pennsylvanian beds are nearly flat lying. An asymmetric fold with one virtually horizontal limb and one nearly vertical limb is present on the east side of the fault. The Sand Canyon area includes a right-stepping bend in the Montosa fault that Hayden (1991) interpreted as a transtensional step. Kinematic indicators in the limestones are typically calcite slickenfibers, but local slickenside striae were noted. The sandstones include excellent exposures of slickensides with thin layers of cataclasite. Slickenlines are distinct and commonly stained with iron. In the vicinity of Sand Canyon an area extending 3 km along strike and as much as 300 m on either side of the fault was studied. Just south of Abo Pass and the Sand Canyon fault bend is the Sais Santa Fe Quarry. The quarry offers a dramatic three-dimensional view of the Proterozoic quartzite and schist in the hanging wall proximal to the Montosa fault. The term "Parker Ranch" refers to a study area along the fault between US–60 and Parker Ranch, where kinematic indicators were found and measured up to 900 m on either side of the fault. At the southern fault tip, the Gallina Well area includes red and white sandstone, mudstone, siltstone, and limestone of the Permian Bursum, Abo, and Yeso Formations. In this area the fault consists of multiple braided strands. A strip 2.5 km along strike and up to 500 m on either side of the fault was examined. The South Spring area, 3.5 km south of the southern fault tip, was also examined for kinematic indicators.

Minor faults associated with the Montosa fault exhibit consistent structural trends. Three populations of reverse faults are present (Fig. 5). The first, and by far the largest, population strikes north to northeast with shallow to steep dips. The second strikes north and dips moderately west. The third population of reverse faults strikes northeast to northwest and is found only in the Sand Canyon and Parker Ranch areas along the central portion of the fault. We also see three populations of dextral strike-slip faults: northeast-striking, moderately to steeply dipping faults that form the largest population; north-striking, steeply dipping faults found only along the central portion of the fault; and northwest-striking faults with moderate to steep dips (Fig. 6). Sinistral strike-slip faults are less common than either reverse or dextral strike-slip faults. Three groups of sinistral strike-slip faults are observed: a northwest- to north-striking set; an east-striking population; and a northeast-striking set that is found only along the central portion of the fault.

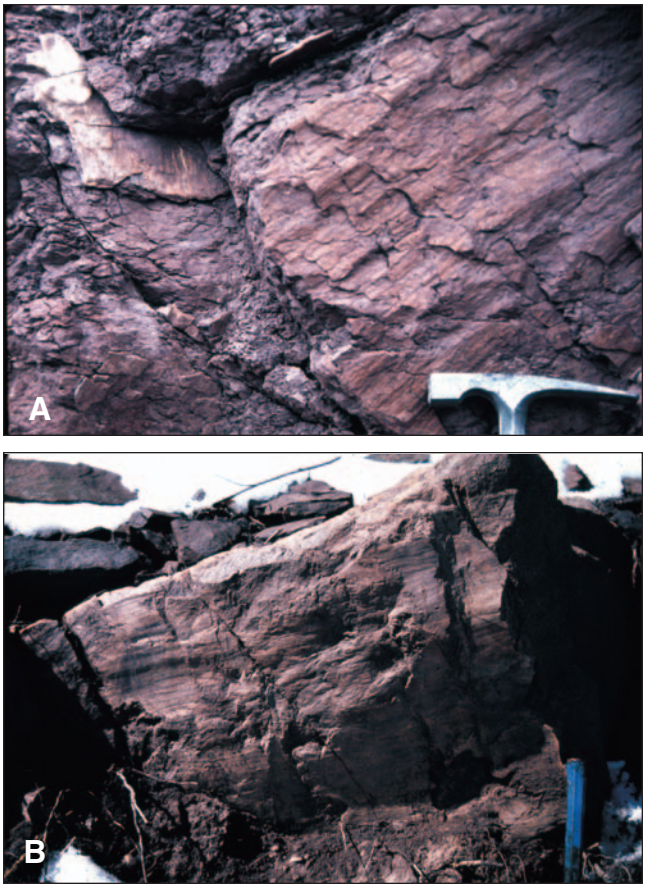

FIGURE 4—(**A**) Two minor faults with calcite slickenfibers in red limy mudstone at Gallina Well. The set on the right records dextral normal oblique-slip movement. The set on the left records normal motion. (**B**) Strike-slip slickenside striae in Permian Abo Sandstone at Cañon Colorado.

A set of conjugate strike-slip faults was found in the field, and an apparent conjugate set of north-northeast-striking minor reverse fault planes is evident in data collected from Gallina Well (Fig. 5). Equal area net plots also suggest conjugate relations between northwest-striking sinistral strike-slip faults and northeast-striking dextral strike-slip faults.

Minor normal faults are common in the southern half of the fault zone (Fig. 7). Minor normal faults observed along the Montosa fault are in many cases parallel to reverse faults (compare Figs. 5, 7). Slickensides that record normal slip locally crosscut dominantly strike-slip slickensides (Fig. 4A).

Fold hinges

The trends of the traces of fold axial planes and fold hinges were measured in the field and from published maps (Wilpolt and Wanek 1951; Myers and McKay 1974; Myers et al. 1981, 1986; Osburn 1984; Colpitts 1986; Brown 1987; Cabezas 1987). Nearly half of the folds are located within 500 m of the fault. Approximately 20% are more than 4 km from

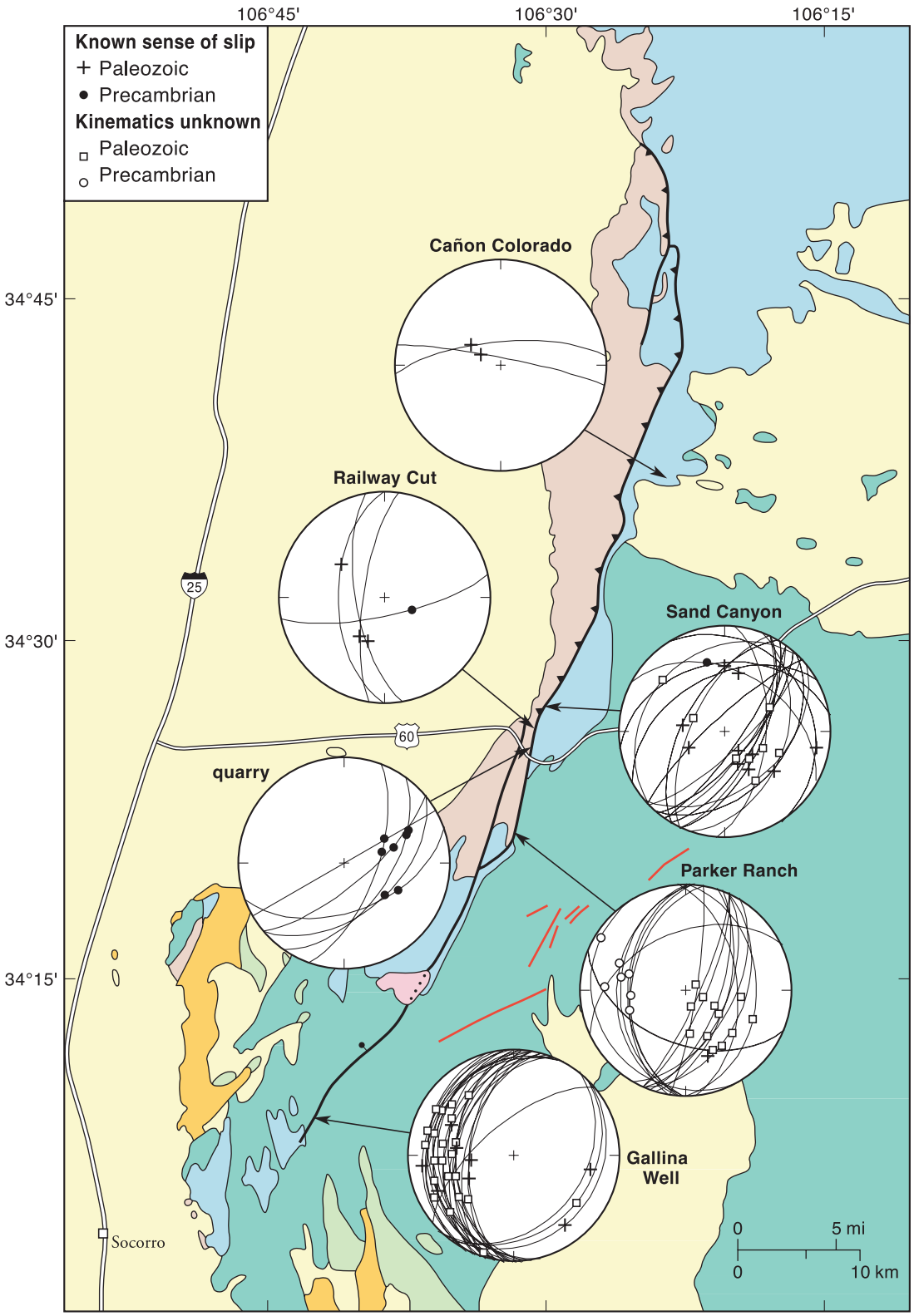

FIGURE 5—Lower hemisphere equal area plots of minor reverse faults and structures with similar orientations but unknown kinematics along the Montosa fault. Key to slickenlines in upper left corner. A line connects each plot to the region in which the data were collected; localities are listed above the plots. The base map for this and Figures 6–9 has been simplified from that shown in Figure 2. **Paleozoic** and **Precambrian** refer to the ages of the host rocks.

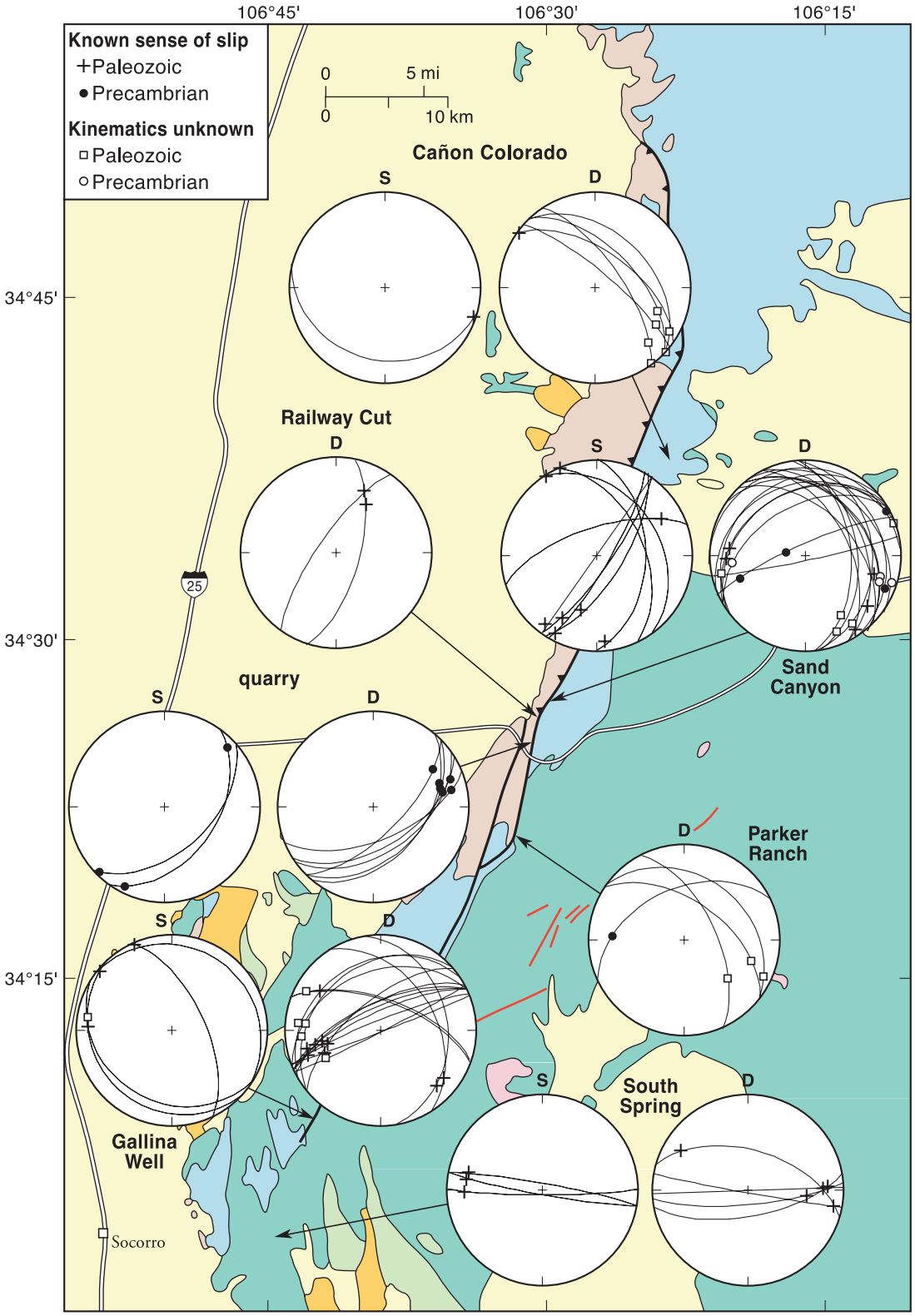

FIGURE 6—Lower hemisphere equal area plots of minor strike-slip faults and structures with similar orientations but unknown kinematics. Key to slickenlines in upper left corner. Plots of dextral strike-slip faults are labeled (**D**), and sinistral strike-slip faults are labeled (**S**). A line connects each pair of plots to the region in which the data were collected; localities are listed above the plots.

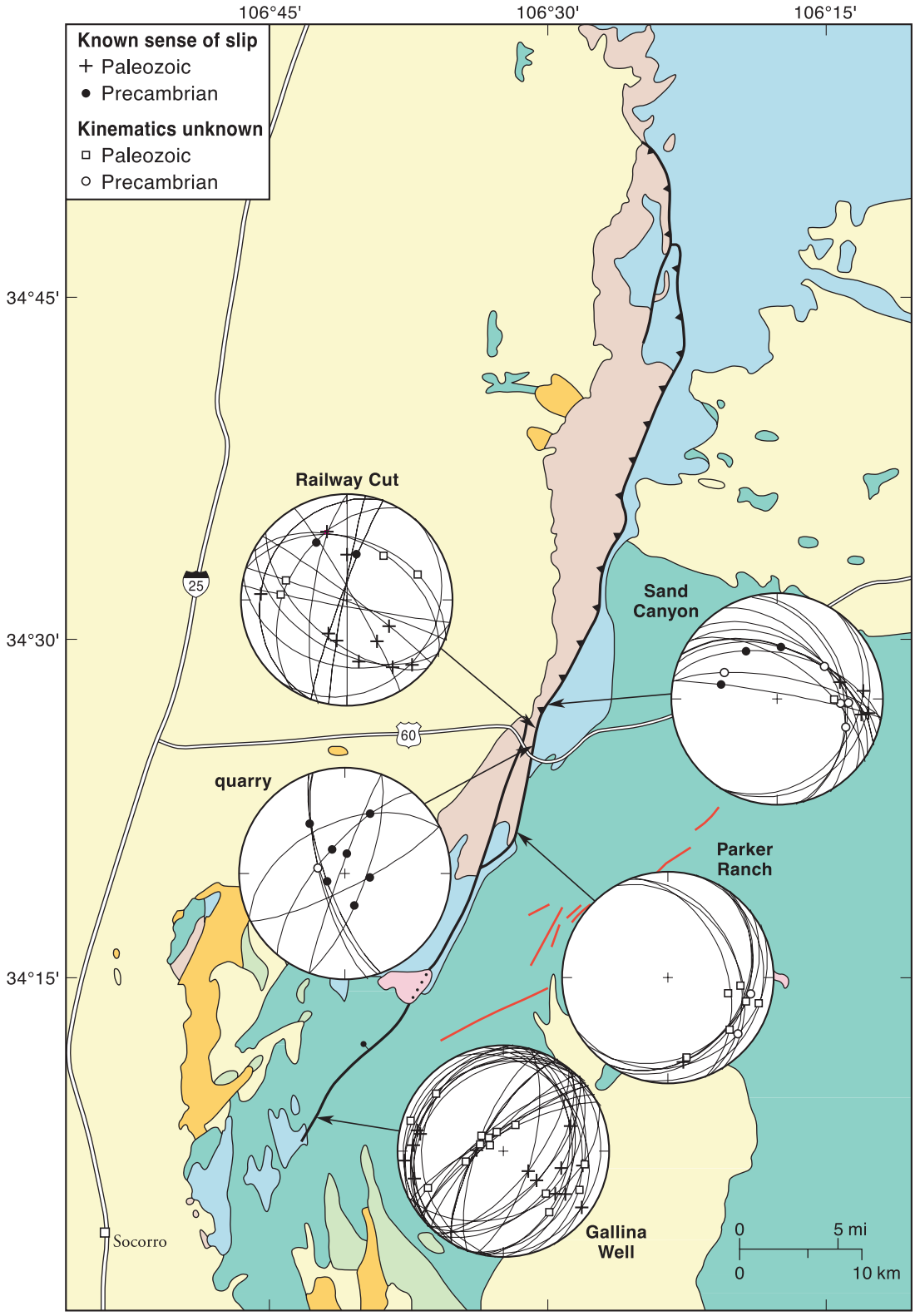

FIGURE 7—Lower hemisphere equal area plots of minor normal faults and structures with similar orientations but unknown kinematics. Key to slickenlines in upper left corner. A line connects each plot to the region in which the data were collected; localities are listed above the plots.

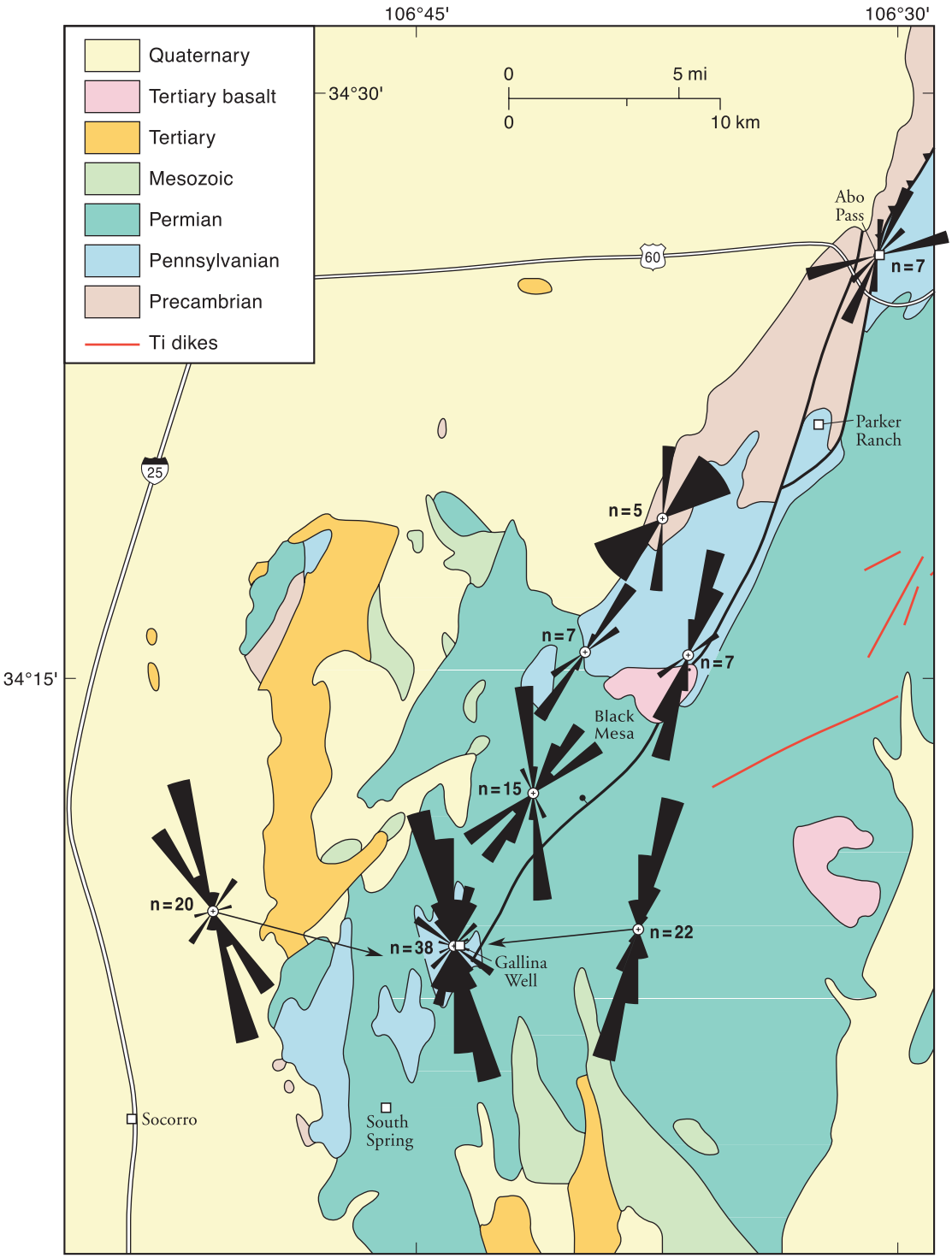

FIGURE 8—Trends of fold hinges along southern half of Montosa fault. Note that the number of fold hinges varies significantly from one area to the next. Rose diagrams are located within the general areas in which data were collected.

the fault. The range and distribution of fold hinge orientations within 0.5 km of the fault is the same as that as far as 9 km from the fault. Most of the fold hinges are nearly horizontal, and all are found in Pennsylvanian and Permian rocks. The fold hinge trends vary in orientation. At Abo Pass they exhibit a bimodal distribution with modes trending N25°E and N70°E (Fig. 8). Near Black Mesa trends vary from N10°W to N60°E with two main modes at N20°E–N40°E and N50°E. Along the southern portion of the fault most of the fold hinges trend N15°E and N15°W, but some range from N80°W to N80°E. Note that the number of fold hinges measured in each area varies significantly (Fig. 8).

Cooling history of the Montosa fault

Procedures

Twenty samples of conglomerate, sandstone, quartzite, granite, and greenstone were collected in eight transects

TABLE 1—Apatite fission-track data from the Montosa fault. ρ_s = spontaneous track density; ρ_i = induced track density (reported induced track density is twice the measured density); ρ_d = track density in muscovite detector covering CN-6 (1.05 ppm), reported value determined from interpolation of values for detectors covering standards at the top and bottom of the reactor packages (fluence gradient correction); number in parentheses is the number of tracks counted for ages and fluence calibration or the number of track measured for lengths. **S.E.** = standard error. $P(\chi)^2$ = Chi-squared probability. **n.d.** = no data. $\lambda_f = 1.551 \times 10^{-10} yr^{-1}$, g = 0.5; * = analyst SK, zeta = 4,882.3 ± 307 for apatite. # = analyst RB, zeta = 5,420. Mean track lengths not corrected for length bias (Laslett et al. 1982).

Sample number	Rock type	Latitude longitude	Elevation (m)	Number of grains dated	ρ_s x 10^5 t/cm^2	ρ_i x 10^6 t/cm^2	ρ_d x 10^5 t/cm^2	Central age (Ma) (± 1 S.E.)	$P(\chi)^2$ (%)	Uranium content (ppm)	Mean track length (µm) (± 1 S.E.)	Standard deviation track length
97PT1	Penn. Sandia sandstone	34°29′50″ 106°28′16″	1975	13	1.1 (53)	2.4 (575)	1.484 (4600)	**33.3 ± 5.0***	99	19	n.d.	
97PT2	Proterozoic Priest Granite	34°29′50″ 106°28′16″	1975	20	1.12 (81)	3.33 (1198)	1.493 (4600)	**24.6 ± 3.0***	40	26		
				29	0.78 (95)	1.66 (2003)	1.7	**21.9 ± 2.3#**	43	17	13.3 ± 1.2 (16)	2.6
97CM2	Proterozoic Blue Springs Schist	34°21′23″ 106°31′43″	1975	20	0.43 (20)	0.57 (134)	1.508 (4600)	**54.7 ± 13.2***	99	4.4	n.d.	
97CM3	Permian Abo fine sandstone	34°21′49″ 106°31′19″	1960	9	1.69 (26)	2.97 (228)	1.47 (4600)	**40.8 ± 8.6***	30	24	n.d.	
				8	0.62 (13)	0.82 (171)	1.7	**35.1 ± 10.1#**	52	8	n.d.	
97BW2	Permian Yeso conglomerate	34°13′04″ 106°37′50″	1765	20	0.46 (31)	1.12 (379)	1.436 (4600)	**28.6 ± 5.4***	93	9	12.8 ± 1.3 (8)	1.9
				20	0.5 (34)	0.93 (634)	1.7	**24.8 ± 4.4#**	88	9	n.d.	
97GW1	Permian Bernal fine sandstone	34°09′10″ 106°41′52″	1730	20	1.52 (74)	4.69 (1141)	1.569 (4600)	**24.8 ± 3.2***	96	35	15.1 ± 0.9 (19)	1.6
97GW2	Permian Bernal arkose	34°09′12″ 106°41′50″	1710	20	1.03 (112)	4.71 (2564)	1.559 (4600)	**16.6 ± 1.8***	85	36	13.1 ± 0.6 (74)	2.6
				26	0.693 (134)	2.38 (4276)	1.7	**14.4 ± 1.4#**	99	26	n.d.	
97GW3	Permian Abo mud peb. cong.	34°09′28″ 106°42′41″	1710	20	1.16 (63)	3.96 (1078)	1.545 (4600)	**22.0 ± 3.0***	80	30	n.d.	

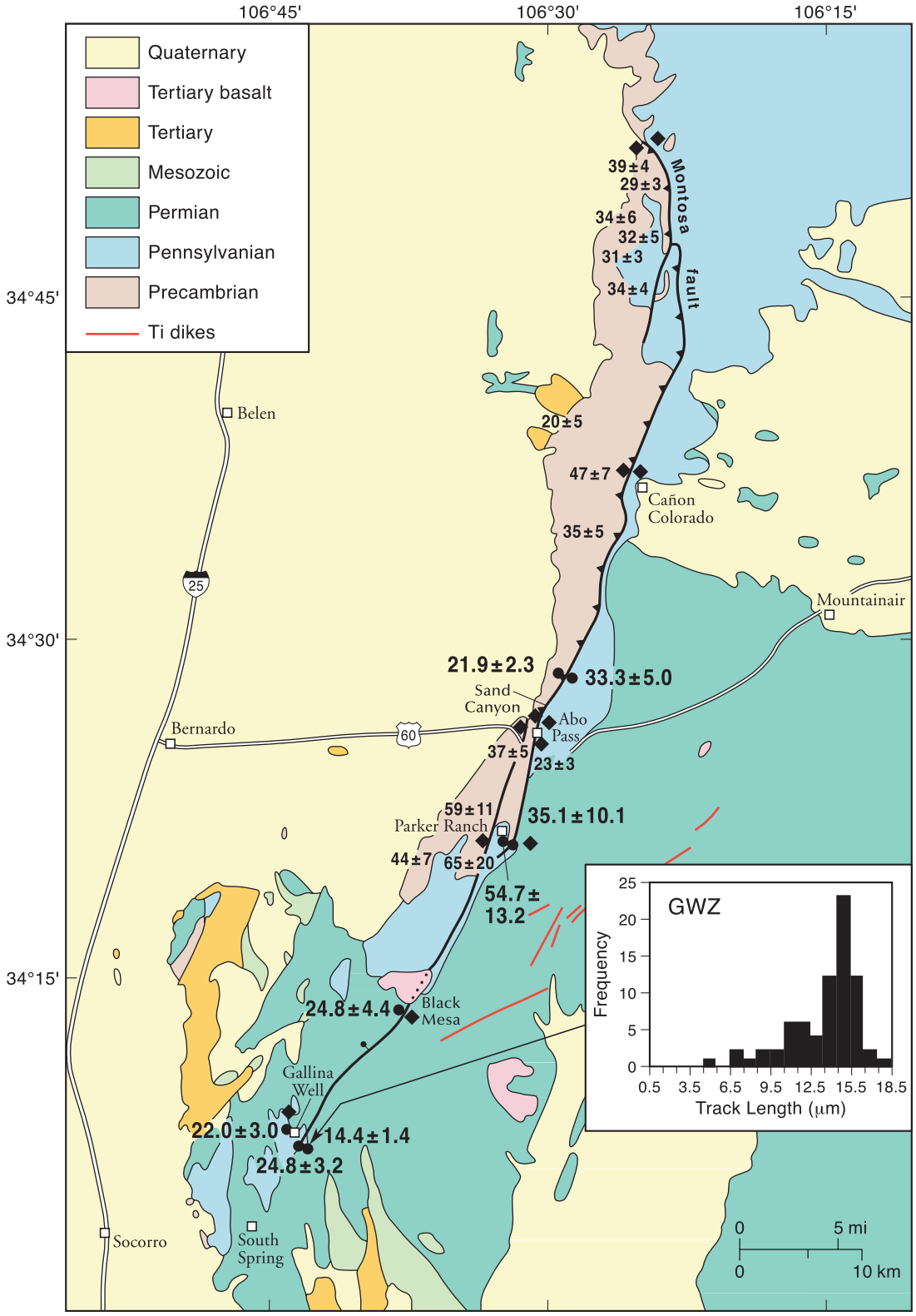

FIGURE 9—New AFT ages and a representative track length distribution from this study. Locations of samples with no apatite are shown with black diamonds. Previous apatite fission-track ages determined by Kelley et al. (1992) in the Los Pinos and Manzano Mountains are also shown (numbers are roughly located above sample locations). Ages are in millions of years.

across the Montosa fault. Samples were crushed and apatite was separated using standard heavy liquid and magnetic techniques. Apatite grains were mounted on glass slides with epoxy, polished, and etched for 25 sec in a 5M solution of nitric acid. Muscovite detectors, which record induced track counts in the external detector method, were attached to each grain mount (Hurford and Green 1983). Samples were assembled in a reactor package with Durango apatite

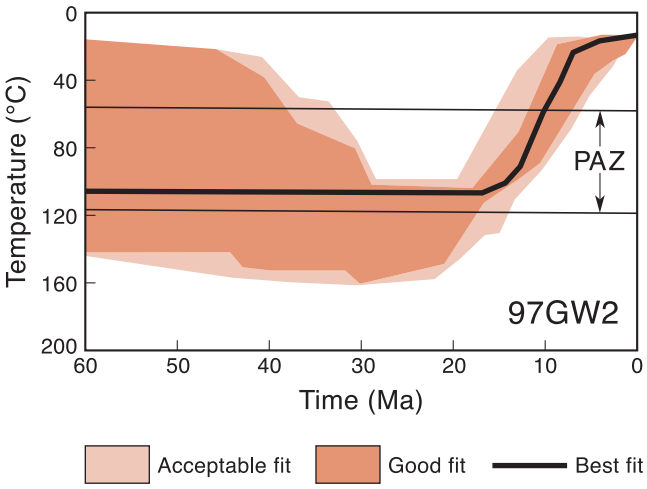

FIGURE 10—Potential thermal histories for sample 97GW2.

(accepted age: 31.4 ± 0.5 Ma) and Corning glass (CN 6) standards and irradiated at the nuclear reactor at Texas A&M University.

The Durango apatite and Corning glass standards were used to calculate zeta, a correction factor that takes into account fluence, procedures, and analyst observation skills (Hurford and Green 1982, 1983). Errors in age were determined using the methods of Galbraith (1984) and Galbraith and Laslett (1985). All samples passed the Chi-squared test, which indicates that only one AFT age population exists in each sample (Galbraith 1981; Green 1981).

Track-length distributions were determined using a microscope with 100X dry objective, drawing tube, and digitizing tablet. Only horizontal, well-etched, confined tracks were measured. Where significant numbers of confined tracks were measured, the AFTSolve© inverse computer model of Ketcham et al. (1999) was used to determine time-temperature curves that are compatible with observed age and track lengths.

Fission-track data

Of the 20 samples collected, eight contained an adequate amount of apatite for analysis. In the southern Manzano Mountains, two samples collected within 3 m of the fault on the footwall and hanging wall, respectively, gave ages of 33 ± 5 and 22 ± 2 Ma (1 standard error; samples 97PT1 and 97PT2; Table 1; Fig. 9). Significant numbers of apatite grains in the Priest pluton of the hanging wall made dating easy, but the footwall Sandia Formation sandstone sample contained only 13 datable grains. Four samples were collected on an age-elevation traverse from Cerro Montoso (just southwest of Parker Ranch; Fig. 2) across the Montosa fault in the northern Los Pinos Mountains. Two of these contained sufficient grains to date and gave ages of 55 ± 13 and 35 ± 10 Ma (Samples 97CM2 in hanging wall and 97CM3 in footwall; Table 1). Low uranium and apatite content resulted in low-quality ages with large standard errors. A sample transect across the fault south of Black Mesa yielded one sample on the hanging wall with sufficient apatite to date (97BW2; Table 1), which gave an AFT age of 25 ± 4 Ma. Three datable samples, collected across the southern fault tip, yielded an age range of 14–25 Ma (97GW1, 97GW2, and 97GW3; Table 1), with the youngest age from within the fault zone and similar ages on either side. In transects with samples on both sides of the fault, ages on either side were essentially the same within error (Fig. 9). The samples from the southern Manzano Mountains yielded AFT ages indicative of cooling in early Oligocene to early Miocene time. AFT ages from the northern and central Los Pinos Mountains indicate cooling in early Eocene to Oligocene time. The samples from the southern Los Pinos Mountains were located in a region of broad valleys, mesas, and cuestas. They record more recent cooling, in late Oligocene to mid-Miocene time.

Track lengths were measured in four samples (97GW1, 97GW2, 97BW2, and 97PT2; Table 1). The mean track lengths range from 15.1 μm for sample 97GW1 to 12.8 μm for sample 97BW2. Only 97GW2 contained enough confined tracks (n = 74) for meaningful track length analysis. The AFT length and age data for this sample, which was collected in the fault zone near Gallina Well at the south end of the fault zone, were modeled using the computer program AFTSolve© to create best-fit temperature histories (Fig. 10). The model was set up to test the sensitivity of the data to cooling due to Laramide deformation. Models assuming uplift and erosion during the Laramide orogeny followed by post-Laramide burial or reheating show that the post-early Miocene cooling is well constrained, but the earlier thermal history is not well known. Thus, this Permian sandstone was heated to temperatures > 110° C before early Miocene time. The AFT data for this sandstone primarily record post-early Miocene cooling, providing little information about any older deformation.

Discussion

Deformation history

Movement on a fault will result in incremental shortening 45° from the slip vector in a plane containing the slip direction, such that the acute angle between the shortening axis and slip vector points in the slip direction. Extension will occur in the same plane, 90° from the shortening direction. For example, north-striking reverse faults, like north-trending upright folds, record east-west shortening and subvertical extension, or crustal thickening. Strike-slip faults do not produce crustal thickening—both shortening and extension directions are subhorizontal. We have determined the directions of maximum incremental shortening and extension from minor faults in the vicinity of the Montosa fault using FaultKin v. 3.8.3 (Allmendinger et al. 1992). This program uses a fault plane, lineation, and slip sense to create a fault plane solution. The principal shortening and extension directions are estimated by bisecting the angle between the nodal planes of the fault plane solution (Marrett and Allmendinger 1990). We subsequently grouped faults that record similar strain to evaluate the deformation history of the damage zone of the Montosa fault, which we compare with deformation in adjacent areas. By analogy with patterns of deformation recorded along faults of known slip (Fig. 3; Chester and Logan 1987; Tavernelli 1998; Ghisetti 2000), we have used these deformation histories to infer the movement history of the Montosa fault. The primary assumptions in this analysis are that: (a) structures that record similar strain were contemporaneous; (b) patterns of deformation are structurally significant; and (c) structures in the damage zone record movement on the Montosa fault. This analysis does not allow an estimate of finite strain or displacement.

Minor reverse and strike-slip faults and folds fall into three distinct groups of strain-compatible structures, which record (1) west-northwest–east-southeast shortening and generally moderately to steeply plunging extension, (2) southwest–northeast shortening and northwest–southeast extension, and (3) north-northwest shortening and west-southwest–east-northeast extension (Figs. 11, 12). Some minor fault planes appear to be strain incompatible. For

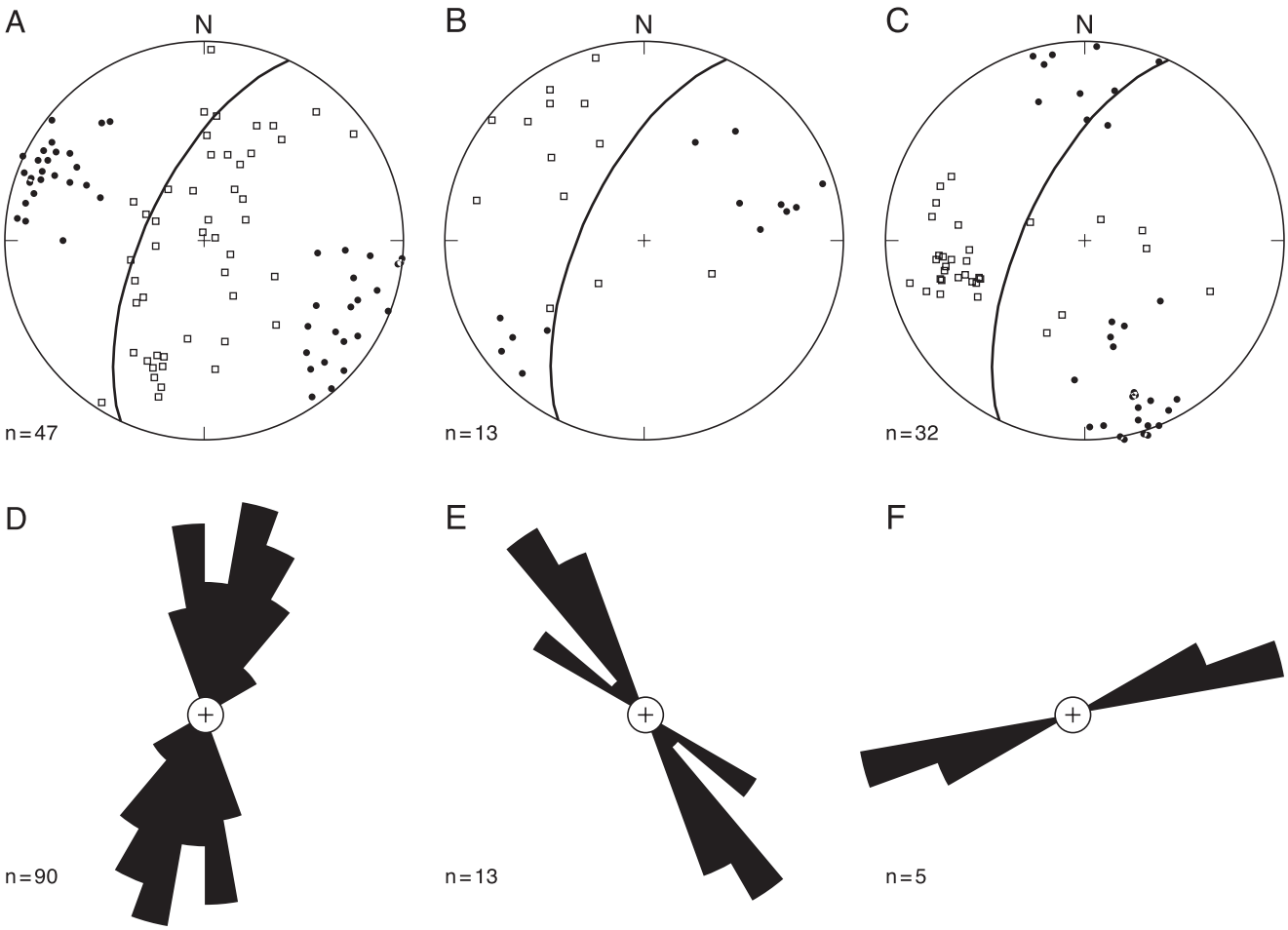

FIGURE 11—Fault-plane solutions determined by FaultKin (Allmendinger et al. 1992) (**A–C**) and rose diagrams of trends of fold hinges (**D–F**). Maximum shortening directions determined from minor faults shown by solid circles; extension directions indicated with squares. (**A**) and (**D**) East-southeast shortening, (**B**) and (**E**) East-northeast shortening, and (**C**) and (**F**) North-northwest shortening. Solid line is trace of common orientation of Montosa fault (N25°E 65°NW).

example, the extension directions calculated from normal faults have the same orientation as the shortening directions determined from some of the reverse and strike-slip faults, indicating that these fault systems were probably not active at the same time (Fig. 13). Note, however, the possibility of normal faults accommodating extension in fold hinges, which could result in similar patterns of deformation (cf. Cooper 2000).

As indicated above, the largest population of minor faults and folds records west-northwest–east-southeast shortening. This deformation is recorded by 21 reverse faults, 21 dextral strike-slip faults, and five sinistral strike-slip faults from every study site except Cañon Colorado, as well as 90 fold hinges from the southern Manzano Mountains to the fault tip (Figs. 11, 12). The minor faults, most of which are located in the damage zone of the Montosa fault, are dominated by equal numbers of reverse and dextral strike-slip faults. These structures indicate that deformation in the damage zone resulted in shortening at a high angle to the main fault. The distribution of fault types indicates that this shortening was accommodated by noncoaxial general shear, resulting in both crustal thickening (recorded by reverse faults) and dextral shear (recorded by dextral strike-slip faults) within the damage zone. Using the approach documented in our Principles and methods section (based on data such as that shown in Fig. 3), we infer that the Montosa fault accommodated west-northwest–east-southeast shortening by dextral-reverse oblique-slip movement. We argue that if the Montosa fault was solely a reverse fault at this time, slip would have been recorded by minor reverse faults and a number of similar-order-of-magnitude dextral and sinistral strike-slip faults in the damage zone. Extension axes associated with this deformation event vary from steeply plunging, showing crustal thickening accommodated by reverse faulting, to shallowly plunging, recording the component of dextral strike-slip motion on the fault (Fig. 11). The relatively large number of structures that record west-northwest–east-southeast shortening suggests either: (1) this was the main deformation event on the Montosa fault; and/or (2) this was the first deformation event on the fault, and structures record deformation before faulting, the initiation and propagation of the fault, and subsequent movement on the fault. In the latter case, we would infer that fault reactivation in subsequent events would not require the development of as many new structures.

Northeast-southwest shortening and northwest-southeast extension are recorded by the smallest number of structures in the area. Structures recording this deformation include: (1) two reverse faults at Gallina Well and the railway cut; (2) four dextral strike-slip faults at the Sais Santa Fe Quarry, Railway Cut, and Sand Canyon; (3) seven sinistral strike-slip faults from Cañon Colorado, Gallina Well, and South Spring; and (4) thirteen fold hinges from the southern end of the fault between Black Mesa and Gallina Well (Figs. 11, 12).

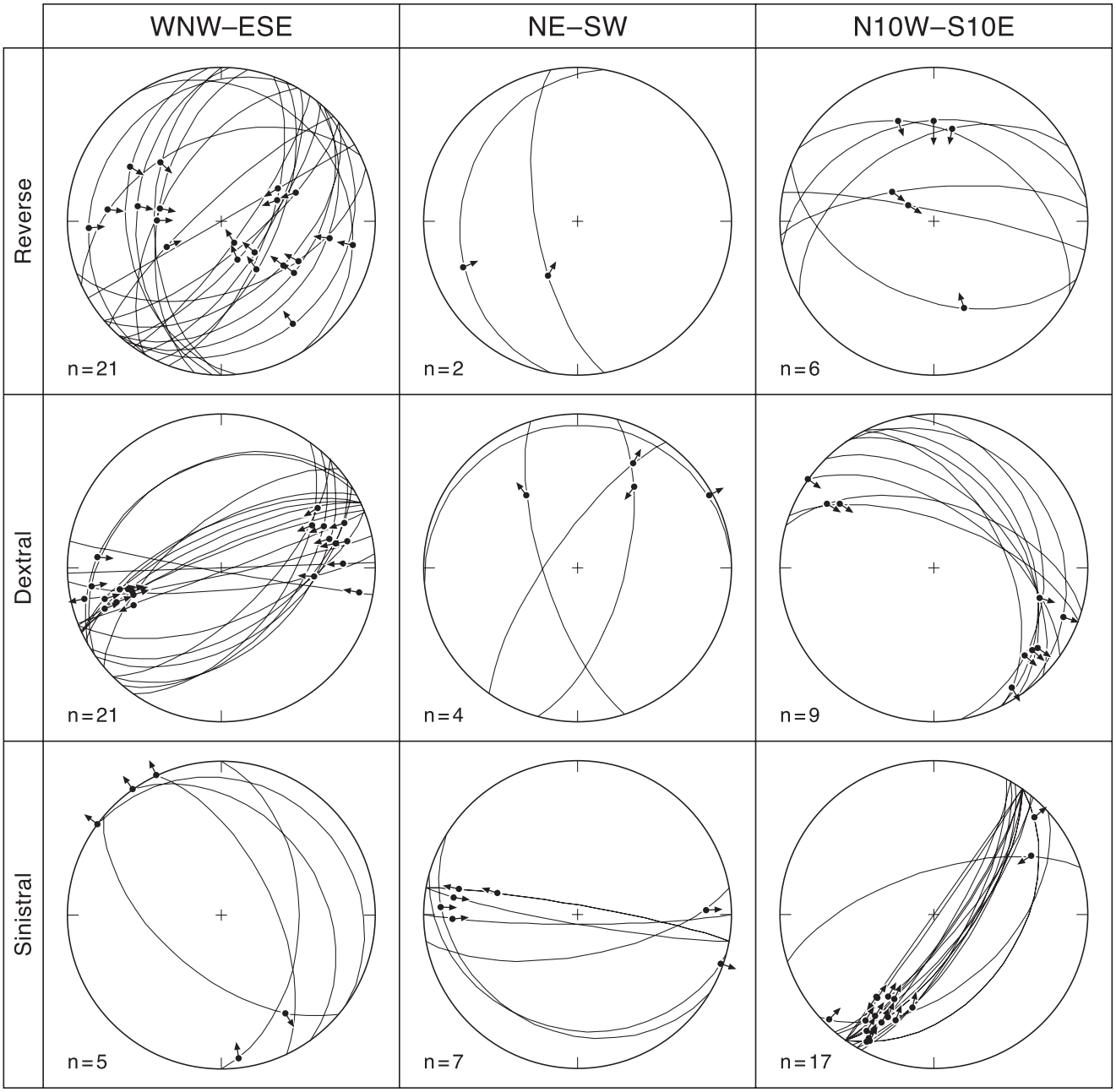

FIGURE 12—Lower hemisphere equal area summary plots of reverse, dextral strike-slip, and sinistral strike-slip faults that record different deformation events. Direction of maximum shortening indicated.

A similar order of magnitude of reverse, dextral, and sinistral strike-slip faults record this deformation. These structures accommodated shortening oblique to the fault without significant crustal thickening, which we interpret as recording dextral strike-slip movement on the Montosa fault.

Evidence of north-northwest–south-southeast shortening, found throughout the study area, includes reverse faults at Cañon Colorado, Sand Canyon, and Parker Ranch; sinistral strike-slip faults at Sand Canyon and the Sais Santa Fe Quarry; dextral faults in Cañon Colorado, Sand Canyon, Gallina Well, and South Spring; and five fold hinges at Abo Pass and Gallina Well (Figs. 11, 12). Sinistral strike-slip faults dominate the minor fault population. These structures indicate that shortening oblique to the Montosa fault was accomplished without significant crustal thickening. The orientations and types of minor faults and folds, and the lack of evidence for crustal thickening, suggest that the Montosa fault accommodated north-northwest–south-southeast shortening with sinistral strike-slip motion.

No evidence was found in the study area to indicate the relative timing of development of the structures described above. Other workers have, however, found crosscutting relationships interpreted to record east-northeast–east compression followed by northeast–north-northeast compression in the Laramide orogeny (Gries 1983; Erslev 2001). Subsequent north-northeast–north compression is constrained to be mid-Tertiary in age, suggesting a transition between Laramide shortening and rift-related extension (Erslev 2001). These maximum principal stress directions are compatible with the shortening and extension directions we have determined from minor fault planes and folds. Because the maximum principal stress is inferred to be

25–30° from the slip direction, assuming a Byerlee coefficient of friction (Byerlee 1978), the trend of the maximum principal stress will only be parallel to the trend of the shortening axis for thrust faults. Thus, for example, northeast-striking sinistral strike-slip faults that record north-northwest–north shortening can be inferred to record north–north-northeast compression assuming an internal coefficient of friction of ~ 0.65. The structures we have documented and the strain they record are therefore compatible with the stresses that Erslev (2001) inferred from minor faults that were mostly outside the damage zones of major faults throughout north-central New Mexico. We therefore suggest that they formed in the order Erslev (2001) proposed. This hypothesis is further tested with data that constrain the timing of deformation in the following sections.

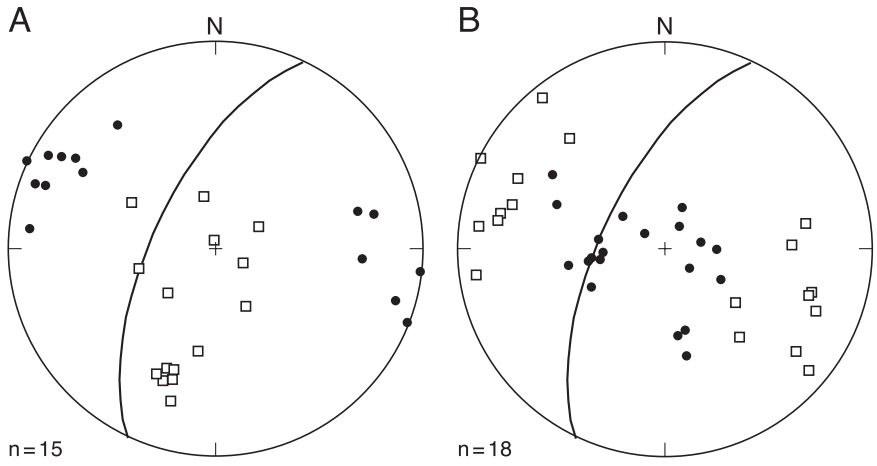

FIGURE 13—Shortening (solid circles) and extension (open squares) directions determined from minor faults in the Gallina Well area using FaultKin (Allmendinger et al. 1992). (**A**) Strain inversion from reverse and dextral fault planes from Gallina Well, indicating east-southeast shortening and crustal thickening. (**B**) Strain inversion from normal fault planes at Gallina Well, showing east-southeast extension, and subvertical shortening, or crustal thinning. Solid line is trace of common orientation of Montosa fault (N25°E 65°NW).

One may well ask why, if our interpretation of the structural history of the Montosa fault is correct, the fault did not initiate as a north-striking thrust fault, because oblique-slip faults are not energetically favorable? Faults and folds are expected to initiate in specific orientations with respect to imposed stresses only if the rock is initially homogeneous with no pre-existing weaknesses and exhibits linear elastic behavior. Rocks are, however, rarely homogeneous. Hayden (1991) noted that the Montosa fault is essentially parallel to the foliation of the Proterozoic basement, and suggested that this preexisting mechanical anisotropy controlled the orientation of the fault. We agree with this interpretation.

Minor normal faults were found in areas bounding the southern half of the fault. Slickenside striae on normal faults are noted to crosscut reverse and strike-slip slickenside striae, and normal planes without crosscutting relationships are in many places parallel to reverse and strike-slip faults in the same area. Thus, normal faults are generally interpreted as reactivated reverse and strike-slip faults. The Montosa fault bounds the eastern edge of the Los Pinos and Manzano Mountains, two rift-flanking ranges. As mentioned previously, a minimum of 90 m of normal separation is recorded locally on the Montosa fault. Reactivation of minor planes is consistent with this evidence that the Montosa fault was reactivated as a normal fault, especially along the southern end. Basalts at Black Mesa (Fig. 2) constrain the timing of normal faulting; they overlie, but are not cut by, the Montosa fault, indicating that it has not been active in the past 3 m.y. (Osburn 1984). Additional timing constraints are discussed below.

Fission-track data—constraints on the timing of fault movement

Three different scenarios that could give rise to similar ages on either side of a fault can be envisioned. First, if the rocks sampled today were faulted at a depth where temperatures were above ~ 110° C, then subsequently cooled by denudation, the AFT ages on either side of the structure would be the same and would record post-faulting denudation. Similarly, the rocks could be faulted at shallow depths, subsequently heated to temperatures above ~ 110° C by a thermal event (volcanism or hydrothermal circulation), then cooled. In this case, the AFT ages would indicate relaxation of isotherms following the thermal event. Finally, small amounts of vertical offset are hard to detect using AFT analysis. In certain situations, such as in the Front Range of Colorado, where the base of the PAZ is preserved, it is possible to detect faults with throw as small as 200 m (Kelley and Chapin 2004 this volume). In areas like the Grand Canyon, which are characterized by low geothermal gradients and relatively slow tectonic processes, it is possible to detect throw on the order of 500 m (Kelley et al. 2004). However, in the Rio Grande rift, where cooling rates are rapid and the geothermal gradient is high, the vertical displacement on a fault must be > 1 km in order to be readily detectable.

The only areas where there is a hint of age difference across the Montosa fault are at Cerro Montoso and in the southern Manzano Mountains. The AFT age of ~ 55 Ma for the Blue Springs Schist on the west side of the fault at Cerro Montoso is comparable to the AFT ages of 44–65 Ma determined for the nearby Los Pinos Granite (Kelley et al. 1992). The AFT age derived from the Permian Abo Sandstone on the east side of the fault is somewhat, but not (within error) significantly younger. Unfortunately, the rock units at this critical locality do not contain confined tracks for track length analysis. Similarly, AFT dates on samples collected across the Priest pluton and the published data of Kelley et al. (1992) along US–60 indicate slightly older ages in the hanging wall compared to the footwall; however, temperatures must have been higher here than at Cerro Montoso during Laramide deformation.

The AFT ages suggest that the Los Pinos block cooled during the Laramide orogeny, and little tectonic activity (as expressed by heating or changes in vertical elevation) has affected this mountain range since that time. In contrast areas to the north and south of this block either were not significantly cooled during Laramide deformation, thus remaining at elevated temperature, or were affected by a post-Laramide heating event. Other lines of geologic evidence may help distinguish between these possibilities. The general decrease in both AFT ages and the number of Laramide structures northward through the Los Pinos–Manzano–Sandia mountain chains (Karlstrom et al. 1999) may indicate that Laramide uplift and erosion decreased toward the north. Later, during Rio Grande rift extension, the Sandia block was most strongly exhumed and the Los

Pinos block was little affected. The Manzano Mountains lie between these extremes, and thus their cooling history may reflect an intermediate deformation history. Little significant age difference across the Montosa fault has been found in the Manzano Mountains. This observation suggests that rocks now exposed at the surface in the vicinity of the Montosa fault were at depths where the temperatures were > ~ 110° C when faulting occurred, and both the footwall and hanging wall blocks cooled during post-Laramide denudation. The Los Pinos fault, a normal fault located west of the Los Pinos and Manzano Mountains, likely accommodated a large portion of the normal displacement resulting from Rio Grande rift formation, and the Montosa fault only accommodated a few hundred meters of normal throw. No evidence for Cenozoic volcanism is exposed at the surface in the Manzano Mountains.

The area south of the Los Pinos block may have had a different thermal history than that to the north due to its closer proximity to middle and late Cenozoic volcanic and intrusive centers. Dikes on Chupadera Mesa and on the Loma de las Cañas are 30–31 Ma (Aldrich et al. 1986). Samples from the southern tip of the Montosa fault reveal younger AFT ages and reflect cooling in late Oligocene to mid-Miocene time. Elevated heat flow associated with volcanism potentially could have removed the evidence for Laramide cooling across the Montosa fault. Mailloux et al. (1999) report 12–18 Ma AFT ages from clasts in Eocene Baca Formation outcrops east of the Rio Grande near Socorro. These authors speculate that a post-Eocene, pre-Miocene hydrothermal system reset AFT ages in the Baca Formation. The young ages at the south end of the Montosa fault are probably not directly related to this hydrothermal anomaly because, in contrast to the Baca Formation, there is no evidence for hydrothermal alteration, such as mineralization or bleaching of the rock.

Low-angle detachment faults are common in the area east of Socorro (Smith 1983). Some of the detachment faults are located a short distance (~ 1.5 km) north of our sample localities at Gallina Well. The origin and time of formation of these features is the subject of considerable debate. In this particular area, the faults are certainly post-Triassic because the allochthonous blocks rest on Triassic red beds. Colpitts (1986), based on his mapping of the area around Gallina Well, was of the opinion that these features are pre- to early Laramide in age because the allochthonous blocks are folded by northeast-trending folds. He also notes that the allochthonous blocks are cut by northeast-striking faults, although in places they rest on northeast-striking faults. He also suggests that detachments at lower elevation east of the Montosa fault can be correlated to a detachment at higher elevation west of the fault. If this correlation is correct, then the detachment was cut by the Montosa fault. Colpitts (1986) suggests that the detachments existed before the Montosa fault developed; however, he did not recognize evidence for normal reactivation of the Montosa fault. Low-angle detachment faults affecting rocks as young as the 28 Ma Vicks Peak Tuff (Smith et al. 1983) have been mapped west of Gallina Well. Although a direct link has yet to be established between the detachment faulting near Gallina Well and that farther west, low-angle faulting during Miocene time could potentially explain the rapid cooling of Permian rocks near the south end of the Montosa fault. More sampling is needed to explore this hypothesis.

We interpret the apatite fission-track data to reflect denudation and cooling of the Manzano and Los Pinos Mountains in the mid-Eocene to mid-Miocene due to late syn- to post-Laramide exhumation and Rio Grande rift extension. Fission-track data across the Montosa fault indicate that, in general, fault movement predated regional cooling, and cooling of both the hanging wall and footwall occurred at approximately the same time.

Timing of deformation

Ancestral Rocky Mountain tectonism took place from the latest Mississippian (Armstrong 1962) to the Early Permian in New Mexico (Peterson 1980; Kottlowski and Stewart 1970). In the Joyita Hills, 20 km west of the Montosa fault, Beck and Johnson (1992) and Beck and Chapin (1994) found north- and northwest-striking faults that record sinistral transtensional faulting during this time period. One subvertical fault, oriented N12°E, cuts the Sandia Formation (Atokan age) but not the Madera Formation (Pennsylvanian, post-Atokan age), constraining the timing of faulting. In the Estancia Basin, a structural basin due east of the Montosa fault, several faults have been interpreted to be Ancestral Rocky Mountain in age (Broadhead 1997). North- to northeast-striking, high-angle faults are the main basin structures. These faults rarely cut the upper members of the Abo Formation but do offset stratigraphically lower beds, which constrains faulting to have occurred before the Early Permian. Because the Montosa fault lies between these two areas and has the same strike as faults in these areas, the possibility that this structure initiated during Ancestral Rocky Mountain deformation must be considered.

The timing of slip along the Montosa fault is constrained by the ages of faulted rocks and the timing of cooling recorded by apatite fission tracks. None of the rocks cut by the Montosa fault are younger than Early Permian in age. All of the structures discussed in the previous sections are found in Proterozoic, Pennsylvanian, and Permian rocks along the fault. Because all of the rocks present, regardless of age, record all three events, faulting must have post-dated deposition, burial, and lithification of the Abo Formation in Early Permian (Wolfcampian) time. Faulting also predated the Oligocene according to apatite fission-track data. Together these data constrain the deformation between Early Permian (Wolfcampian) and mid-Cenozoic (Oligocene) time. The Montosa fault therefore could have been active late in the Ancestral Rocky Mountain deformation event. It is more likely, given the time required for the multi-stage history recorded by structures in the area that deformation initiated during the Laramide orogeny. Furthermore, the lack of evidence for (1) dramatic changes in stratigraphic thickness across the fault, (2) sediment provenance or paleocurrents suggesting sources in the Manzano or Los Pinos Mountains, (3) angular unconformities in the Pennsylvanian–Permian section (Myers 1982; Stark and Dapples 1946), and (4) structural evidence for deformation of poorly lithified sediment (cf. Heynekamp et al. 1999; Rawling and Goodwin 2003) preclude significant vertical displacement during Pennsylvanian–Permian sedimentation, although minor movement cannot be ruled out.

Magnitude of dextral strike-slip motion

We began this paper by noting the controversy regarding the magnitude of dextral strike-slip motion on north-striking faults east of the Colorado Plateau. Our fault and fold data lead us to conclude that the Montosa fault initiated as a reverse structure with a dextral component of movement and was reactivated first as a dextral strike-slip fault, then as a sinistral strike-slip fault, and finally as a normal fault. These data do not, however, help us to constrain the magnitude of dextral strike-slip movement. In order to evaluate this, we consider first the possibility of strain partitioning and second evidence for deformation in fault steps.

As mentioned earlier, strain may be partitioned during oblique convergence, such that strike-slip deformation is localized within a single fault zone and shortening is accom-

modated in surrounding areas. The best-studied example of this phenomenon is the San Andreas fault (e.g., Mount and Suppe 1992; Teyssier et al. 1995; Tavarnelli 1998). In this case, structures recording deformation within the damage zone are very different from those more than ~ 1 km from the fault (Fig. 3). One approach to evaluating the possibility of similar strain partitioning between the Montosa fault and surrounding areas is therefore to compare structures within the damage zone with those farther from the fault. Most of the minor faults we examined are situated within 300 m of the Montosa fault, but as noted previously, others are further away. Most of the folds examined were within 3 km, and a few were as much as 14 km from the fault. These structures all record the same deformation history, regardless of distance from the fault, suggesting that deformation was not partitioned between strike-slip movement on the fault and shortening accommodated by thrust faults and folds farther from the fault.

Right steps are common along the Montosa fault. They should have acted as releasing bends during dextral strike-slip, in which case they would record extension. The relative magnitude of strike-slip motion should be proportional to extension in these right bends. Hayden (1991) hypothesized that the fault bend at Abo Pass acted as a transtensional step. However, we observed no extensional structures within the right steps of the Montosa fault, and the upturned beds just south of Cerro Montoso record a component of reverse motion in the fault step. The latter could have been produced during sinistral strike-slip motion on the fault, emphasizing the difficulty in determining the displacement history of a long-lived fault system. Significant reverse motion is also recorded by stratigraphic separation along the main fault. At a larger scale, the northeast-striking Tijeras–Cañoncito fault zone may be considered a right step between the Montosa and Picuris–Pecos faults (Cather 1992). The Tijeras–Cañoncito fault zone records dominantly right-lateral strike-slip movement, but also includes evidence of north-side-down normal motion (Abbott et al. 1995; Abbott et al. 2004 this volume). These data are consistent with both reverse and right-lateral motion, respectively, on the Montosa fault, and again offer no evidence of the style of strain partitioning exhibited by the San Andreas fault.

Conclusions

Minor faults and folds indicate a two-stage Laramide deformation history, with dextral reverse (west-northwest shortening) followed by dextral strike-slip (northeast shortening) motion on the Montosa fault. The prevalence of structures that record west-northwest shortening is consistent with initiation of the fault as a dextral reverse fault; we agree with Hayden (1991) that the foliation in the Proterozoic basement determined the initial orientation of the fault. Stratigraphic separation records a minimum of 670 m of reverse displacement along the central portion of the fault, but the magnitude of strike-slip displacement cannot be determined. It was, however, apparently insufficient to produce extensional structures in right steps in the fault.

We agree with Erslev (2001) that north-northwest–south-southeast shortening without crustal thickening may represent the transition between Laramide shortening and Rio Grande rift extension. The Montosa fault accommodated sinistral strike-slip motion during this transition. At least part of the Montosa fault was reactivated as a normal fault, and at least 160 m of normal separation is evident south of Black Mesa.

AFT analysis of samples along the Montosa fault in the lower elevations of the Manzano and Los Pinos Mountains indicates cooling in Eocene to mid-Miocene time due to exhumation during the Laramide orogeny and Rio Grande rift extension. This interpretation agrees with previous work. Samples from the southern tip of the fault show a 14–25 Ma age range indicating cooling in the late Oligocene to mid-Miocene, possibly following a thermal event of uncertain origin or related to a previously unrecognized episode of low-angle mid-Miocene faulting. AFT transects do not show significant age variations across the Montosa fault. Reverse faulting during the Laramide orogeny is not convincingly recorded in the AFT data because (1) faulting occurred when the rocks were at temperatures above ~ 110 °C; or (2) the rocks were reheated in post-Laramide time. Normal faulting due to Rio Grande rift extension also occurred at temperatures above ~ 110 °C and is not recorded in the ages across the fault, or displacement was too minimal to see. In all areas examined in this study except in the Los Pinos block, the later thermal effects of Rio Grande rift formation have erased any possible Laramide history recorded by the apatite fission tracks.

As mentioned in the introduction, some workers believe that the magnitude of dextral strike-slip across New Mexico is limited to less than 20 km (e.g., Woodward et al. 1997); others suggest that more than 33 km of separation occurred across faults with a northerly strike during the Laramide orogeny (Karlstrom and Daniel 1993; Cather 1999). Although our work has clarified the deformation history of the Montosa fault, we have not determined the magnitude of right-lateral strike-slip movement on the fault, although our work does suggest that it was not sufficient to develop significant extensional structures within right steps in the fault. This observation does not, however, help resolve this controversy. Bauer and Ralser (1995) documented evidence that the Picuris–Pecos fault was part of a Laramide-age transpressional flower structure. As the easternmost brittle Laramide structure at this latitude, the Montosa fault could be part of a similar structure, which records a greater component of dip-slip movement at its margins. If this were the case, the faults that accommodated the better part of the strike-slip motion would be buried in the rift.

Acknowledgments

R. Behr thanks the New Mexico, Wyoming, and Four Corners Geological Societies for financial support of this project. This work could not have been completed without the field vehicle and access to crushing and mineral separation facilities provided by the New Mexico Bureau of Geology and Mineral Resources and the New Mexico Argon Lab. Apatite samples were irradiated at Texas A&M under the DOE reactor share program. The Sevilleta National Wildlife Refuge allowed access to critical outcrops. Thanks to Dave Johnson for valuable stratigraphic information, and Erwin Melis and Doug Jones for assistance in the field. Jack Keegan provided a Brunton compass. Finally, we thank our reviewers: Steve Cather, Scott Cooper, Eric Erslev, Marta Hemmerich, J. Matthew Herrin, Charles Naeser, and Clay Smith.

References

Abbott, J. C., 1995, Constraints on the deformation history of the Tijeras–Cañoncito fault system, north central New Mexico: Unpublished M.S. thesis, New Mexico Institute of Mining and Technology, 161 pp.

Abbott, J. C., and Goodwin, L. B., 1995, A spectacular exposure of the Tijeras fault, with evidence for Quaternary motion; *in* Bauer, P. W., Kues, B. S., Dunbar, N. W., Karlstrom, K. E., and Harrison, B. (eds.), Geology of the Santa Fe region: New Mexico Geological Society, Guidebook 46, pp. 117–125.

Abbott, J. C., Goodwin, L. B., Kelley, S. A., and Maynard, S., 2004 this volume, The anatomy of a long-lived fault system: structural and thermochronologic evidence for Laramide to Quaternary

activity on the Tijeras–Cañoncito fault system, New Mexico; *in* Cather, S. M., McIntosh, W. C., and Kelley, S. A. (eds.), Tectonics, geochronlolgy, and volcanism in the Southern Rocky Mountains and Rio Grande rift: New Mexico Bureau of Geology and Mineral Resources, Bulletin 160, pp. 113–138.

Aldrich, M. J., Jr., Chapin, C. E., and Laughlin, A. W., 1986, Stress history and tectonic development of the Rio Grande rift, New Mexico: Journal of Geophysical Research, v. 91, no. B6, pp. 6199–6211.

Allmendinger, R. W., Marrett, R. A., and Cladouhos, T., 1992, FaultKin. Available at http://www.geo.cornell.edu/geology/faculty/RWA/, accessed Feb. 10, 2004.

Armstrong, A. K., 1962, Stratigraphy and paleontology of the Mississippian System in southwestern New Mexico and adjacent southeastern Arizona: New Mexico Bureau of Mines and Mineral Resources, Memoir 8, 99 pp.

Baltz, E. H., 1967, Stratigraphic and regional tectonic implications of part of the Upper Cretaceous and Tertiary rocks, east central San Juan Basin, New Mexico: U.S. Geological Survey, Professional Paper 552, 101 pp.

Bauer, P., and Ralser, S., 1995, The Picuris–Pecos fault—repeatedly reactivated, from Proterozoic(?) to Neogene; *in* Bauer, P. W., Kues, B. S., Dunbar, N. W., Karlstrom, K. E., and Harrison, B. (eds.), Geology of the Santa Fe region: New Mexico Geological Society, Guidebook 46, pp. 111–115.

Beck, W. C., and Chapin, C. E., 1994, Structural and tectonic evolution of the Joyita Hills, central New Mexico—implications of basement control on Rio Grande rift; *in* Keller, G. R., and Cather, S. M. (eds.), Basins of the Rio Grande rift—structure, stratigraphy, and tectonic setting: Geological Society of America, Special Paper 291, pp. 187–205.

Beck, W. C., and Johnson, D. B., 1992, New fusulinid data and multiple episodes of ancestral Rocky Mountain deformation in the Joyita Hills, Socorro County, New Mexico: New Mexico Geology, v. 14, no. 3, pp. 53–59.

Broadhead, R. F., 1997, Subsurface geology and oil and gas potential of Estancia Basin, New Mexico: New Mexico Bureau of Mines and Mineral Resources, Bulletin 157, 54 pp.

Brown, K. B., 1987, Geology of the southern Cañoncito de la Uva area, Socorro County, New Mexico: Unpublished M.S. thesis, New Mexico Institute of Mining and Technology, 89 pp.

Byerlee, J. D., 1978, Friction of rock: Pure and Applied Geophysics, v. 116, no. 4–5, pp. 615–626.

Cabezas, P., 1987, Stratigraphie et tectonique des deux bordures de rift du Rio Grande dans la region de Socorro. Unpublished Ph.D. dissertation, L'Universite de Nice, 188 pp.

Cabezas, P., 1991, The southern Rocky Mountains in west-central New Mexico–Laramide structures and their impact on the Rio Grande rift extension: New Mexico Geology, v. 13, no. 2, pp. 25–37.

Carlson, W. D., Donelick, R. A., and Ketcham, R. A., 1999, Variability of apatite fission-track annealing kinetics—I. Experimental results: American Mineralogist, v. 84, pp. 1213–1223.

Castillo, D. A., Hickman, S. H., Choi, X., 1997, High shear stress segment along the San Andreas fault: Near-field stress observations in the Carrizo plain area (abs.): Eos, Transactions, v. 78, no. 46, p. 677.

Cather, S. M., 1992, Suggested revisions to the Tertiary tectonic history of north-central New Mexico; *in* Lucas, S. G., Kues, B. S., Williamson, T. E., and Hunt, A. P. (eds.), San Juan Basin IV: New Mexico Geological Society, Guidebook 43, pp.109–122.

Cather, S. M., 1983, Laramide Sierra uplift: Evidence for a major prerift uplift in central and southern New Mexico; *in* Chapin, C. E., and Callender, J. F. (eds.), Socorro region II: New Mexico Geological Society, Guidebook 34, pp. 99–102.

Cather, S. M., 1999, Implications of Jurassic, Cretaceous, and Proterozoic piercing lines for Laramide oblique-slip faulting in New Mexico and rotation of the Colorado Plateau: Geological Society of America, Bulletin, v. 111, pp. 849–868.

Cather, S. M., and Johnson, B. D., 1986, Eocene depositional systems and tectonic framework of west-central New Mexico and eastern Arizona; *in* Peterson, J. A. (ed.), Paleotectonics and sedimentation in the Rocky Mountain region of the United States: American Association of Petroleum Geologists, Memoir 41, pp. 623–652.

Chapin, C. E., and Cather, S. M., 1981, Eocene tectonics and sedimentation in the Colorado Plateau–Rocky Mountain area; *in* Dickinson, W. R., and Payne, M. D. (eds.), Relations of tectonics to ore deposits in the southern Cordillera: Arizona Geological Society, Digest, v. 14, pp. 173–198.

Chester, F. M., and Logan, J. M., 1987, Composite planar fabric of gouge from the Punchbowl fault, California: Journal of Structural Geology, v. 9, no. 5–6, pp. 621–634.

Colpitts, R. M., Jr., 1986, Geology of the Sierra de la Cruz area, Socorro County, New Mexico: New Mexico Bureau of Mines and Mineral Resources, Open-file Report 244, 166 pp.

Coney, P. J., and Reynolds, S. J., 1977, Cordilleran Benioff zones: Nature, v. 270, no. 5636, pp. 403–406.

Cooper, S. P., 2000, Deformation within a basement-cored anticline—Teapot Dome, Wyoming: Unpublished M.S. thesis, New Mexico Institute of Mining and Technology, 274 pp.

Crowley, K. D., Cameron, M., and Schaefer, R. L., 1991, Experimental studies of annealing of etched fission tracks in fluorapatite: Geochemica et Cosmochemica Acta, v. 55, pp. 1449–1465.

de Voogd, B., Brown, L. D., and Merey, C., 1986, Nature of the eastern boundary of the Rio Grande rift from COCORP surveys in the Albuquerque Basin, New Mexico: Journal of Geophysical Research, v. 91, no. 6, pp. 6305–6320.

Dickinson, W. R., and Snyder, W. S., 1978, Plate tectonics of the Laramide orogeny; *in* Matthews, V. (ed.), Laramide folding associated with basement block faulting in the western United States: Geological Society of America, Memoir 151, pp. 355–365.

Erslev, E. A., 2001, Multistage, multi-directional Tertiary shortening and compression in north-central New Mexico: Geological Society of America, Bulletin, v. 113, no. 1, pp. 63–74.

Ferguson, C. A., Timmons, J. M., Pazzaglia, F. J., Karlstrom, K. E., Osburn, G. R., and Bauer, P. W., 1999, Geology of Sandia Park quadrangle, Bernalillo and Sandoval Counties, New Mexico: New Mexico Bureau of Mines and Mineral Resources, Open-file Geologic Map OF-GM-1, scale 1:24,000.

Fitzgerald, P. G., Sorkhabi, R. B., Redfield, T. F., and Stump, E., 1995, Uplift and denudation of the central Alaska Range—a case study in the use of apatite fission-track thermochronology to determine absolute uplift parameters: Journal of Geophysical Research, v. 100, pp. 20,175–20,191.

Fleuty, M. J., 1975, Slickensides and slickenlines: Geology Magazine, v. 112, no. 3, pp. 319–322.

Galbraith, R. F., 1981, On statistical models for fission-track counts: Mathematical Geology, v. 13, pp. 471–438.

Galbraith, R. F., 1984, On statistical estimation of fission-track dating: Mathematical Geology, v. 16, no. 7, pp. 653–669.

Galbraith, R. F., and Laslett, G. M., 1985, Some remarks on statistical estimation of fission-track dating: Nuclear Tracks, v. 10, no. 3, pp. 361–363.

Gallagher, K., Brown, R., and Johnson, C., 1998, Fission track analysis and its application to geological problems: Annual Review Earth Planetary Sciences, v. 26, pp. 519–572.

Ghisetti, F., 2000, Slip partitioning and deformation cycles close to major faults in southern California—evidence from small-scale faults: Tectonics, v. 19, no. 1, pp. 25–43.

Gleadow, A. J. W., Duddy, I. R., Green, P. F., and Hegarty, K. A., 1986, Fission track lengths in the apatite annealing zone and the interpretation of mixed ages: Earth and Planetary Science Letters, v. 78, no. 2–3, pp. 245–254.

Green, P. F., 1981, A new look at statistics in fission-track dating. Nuclear Tracks, v. 5, pp. 77–86.

Green, P. F., Duddy, I. R., Gleadow, A. J. W., Tingate, P. R., and Laslett, G. M., 1986, Thermal annealing of fission tracks in apatite, part 1. A qualitative description: Chemical Geology, Isotope Geoscience Section, v. 59, no. 4, pp. 237–253.

Gries, R. R., 1983, North-south compression of Rocky Mountain foreland structures; *in* Lowell, J. D. (ed.), Foreland basins and uplifts: Rocky Mountain Association of Geologists, pp. 9–32.

Hamilton, W., 1981, Plate-tectonic mechanisms of Laramide deformation; *in* Boyd, D. W., and Lillegraven, J. A. (eds.), Rocky Mountain foreland basement tectonics: University of Wyoming, Contributions to Geology, v. 19, no. 2, pp. 87–92.

Hayden, S. N., 1991, Dextral oblique-slip deformation along the Montosa fault zone at Abo Pass, Valencia and Socorro Counties, New Mexico (abs.): New Mexico Geology, v. 13, no. 2, p. 64.

Heynekamp, M. R., Goodwin, L. B., Mozley, P. S ., and Haneberg, W. C., 1999, Controls on fault-zone architecture in poorly lithified sediments, Rio Grande rift, New Mexico—implications for fault-

zone permeability and fluid flow; *in* Haneberg, W. C., Mozley, P. S., Moore, J. C., and Goodwin, L. B. (eds.), Faults and subsurface fluid flow in the shallow crust: American Geophysical Union, Monograph 113, pp. 27–49.

Hurford, A. J., and Green, P. F., 1982, A user's guide to fission-track dating calibration: Earth and Planetary Science Letters, v. 59, no. 2, pp. 343–354.

Hurford, A. J., and Green, P. F., 1983, The zeta age calibration of fission-track dating: Isotope Geoscience, v. 1, no. 5, pp. 285–317.

Ingersoll, R. A., 2000, Implications of Jurassic, Cretaceous, and Proterozoic piercing lines for Laramide oblique-slip faulting in New Mexico and rotation of the Colorado Plateau—discussion: Geological Society of America, Bulletin, v. 112, no. 5, pp. 796–797.

Karlstrom, K. E., and Daniel, C. G., 1993, Restoration of Laramide right-lateral strike slip in northern New Mexico by using Proterozoic piercing points—tectonic implications from the Proterozoic to the Cenozoic: Geology, v. 21, no. 12, pp. 1139–1142.

Karlstrom, K. E., Cather, S. M., Kelley, S. A., Heizler, M. T., Pazzaglia, F. J., and Roy, M., 1999, Sandia Mountains and Rio Grande rift—ancestry of structures and history of deformation; *in* Pazzaglia, F. J., and Lucas, S. G. (eds.), Albuquerque geology: New Mexico Geological Society, Guidebook 50, pp. 155–166.

Keith, S. B., 1978, Paleosubduction geometries inferred from Cretaceous and Tertiary magmatic patterns in southwestern North America: Geology, v. 6, no. 9, pp. 516–521.

Kelley, S. A., and Chapin, C. E., 2004 this volume, Denudational histories of the Front Range and Wet Mountains, Colorado, based on apatite fission-track thermochronology; *in* Cather, S. M., McIntosh, W. C., and Kelley, S. A. (eds.), Tectonics, geochronology, and volcanism in the Southern Rocky Mountains and Rio Grande rift: New Mexico Bureau of Geology and Mineral Resources, Bulletin 160, pp. 41–78.

Kelley, S. A., Chapin, C. E., and Corrigan, J., 1992, Late Mesozoic to Cenozoic cooling histories of the flanks of the northern and central Rio Grande rift, Colorado and New Mexico: New Mexico Bureau of Mines and Mineral Resources, Bulletin 145, 39 pp.

Kelley, S. A., Chapin, C. E ., and Karlstrom, K. E., 2004, Laramide cooling histories of the Grand Canyon, Arizona, and the Front Range, Colorado, determined from apatite fission-track thermochronology; *in* Young, R. A., and Spamer, E. E. (eds.), The Colorado River—origin and evolution: Grand Canyon Association, Monograph 12, pp. 37–42.

Kelley, V. C., 1977, Geology of the Albuquerque Basin, New Mexico: New Mexico Bureau of Mines and Mineral Resources, Memoir 33, 60 pp.

Kelley, V. C., and Northrop, S. A., 1975, Geology of Sandia Mountains and vicinity, New Mexico: New Mexico Bureau of Mines and Mineral Resources, Memoir 29, 136 pp.

Ketcham, R. A., Donelick, R. A., and Carlson, W. D., 1999, Variability of apatite fission-track annealing kinetics—III. Extrapolation to geological time scales: American Mineralogist, v. 84, pp. 1235–1255.

Knepper, D. H., and Maars, R. W., 1971, Geological development of the Bonanza–San Luis Valley–Sangre de Cristo area, south central Colorado; *in* James, H. L. (ed.), San Luis Basin: New Mexico Geological Society, Guidebook 22, pp. 249–264.

Kottlowski, F. E., and Stewart, W .J., 1970, The Wolfcampian Joyita Uplift in central New Mexico: New Mexico Bureau of Mines and Mineral Resources, Memoir 23, Part I, 31 pp.

Lachenbruch, A. H., and Sass, J. H., 1980, Heat flow and energetics of the San Andreas fault zone: Journal of Geophysical Research, v. 96, no. 11, pp. 8369–8389.

Laslett, G. M., Kendall, W. S., Gleadow, A. J. W., and Duddy, I. R., 1982, Bias in measurement of fission-track length distribution: Nuclear Tracks, v. 6, no. 2–3, pp. 79–85.

Laslett, G. M., Green, P. F., Duddy, I. R., and Gleadow, A. J. W., 1987, Thermal annealing of fission tracks in apatite, 2. A quantitative analysis: Chemical Geology, Isotope Geoscience Section, v. 65, pp. 1–13.

Lisenbee, A. L., Woodward, L. A., and Connolly, J. R., 1979, Tijeras–Cañoncito fault system—a major zone of recurrent movement in north-central New Mexico; *in* Ingersoll, R. V., Woodward, L. A., and James, H. L. (eds.), Santa Fe country: New Mexico Geological Society, Guidebook 30, pp. 89–99.

Livaccari, R. F., 1991, Role of crustal thickening and extensional collapse in the tectonic evolution of the Sevier–Laramide orogeny, western United States: Geology, v. 19, no. 11, pp. 1104–1107.

Lucas, S. G., Anderson, O. J., and Black, B. A., 2000, Implications of Jurassic, Cretaceous, and Proterozoic piercing lines for Laramide oblique-slip faulting in New Mexico and rotation of the Colorado Plateau—discussion: Geological Society of America, Bulletin, v. 112, no. 5, pp. 789–790.

Mailloux, B. J., Person, M., Kelley, S. A., Dunbar, N. W., Cather, S. M., Strayer, L., and Hudleston, P., 1999, Tectonic controls of the hydrology of the Rio Grande rift, New Mexico: Water Resources Research, v. 35, no. 9, pp. 2641–2659.

Marrett, R., and Allmendinger, R. W., 1990, Kinematic analysis of fault slip-data: Journal of Structural Geology, v. 12, pp. 973–986.

Maxson, J., and Tikoff, B., 1996, Hit-and-run collision model for the Laramide orogeny, western United States: Geology, v. 24, no. 3, pp. 968–972.

Miller, J. P., Montgomery, A., and Sutherland, P. K., 1963, Geology of part of the southern Sangre de Cristo Mountains, New Mexico: New Mexico Bureau of Mines and Mineral Resources, Memoir 11, 106 pp.

Mount, V. S., and Suppe, J., 1992, Present-day stress orientations adjacent to active strike-slip faults—California and Sumatra: Journal of Geophysical Research, v. 97, no. 8, pp. 11,995–12,013.

Myers, D. A., 1977, Geologic map of the Scholle quadrangle, Socorro, Valencia, and Torrance Counties, New Mexico: U.S. Geological Survey, Geologic Quadrangle Map GQ 1412, scale 1:24,000.

Myers, D. A., 1982, Stratigraphic summary of the Pennsylvanian and Lower Permian rocks, Manzano Mountains, New Mexico; *in* Wells, S. G., Grambling, J. A., and Callender, J. F. (eds.), Western slope: New Mexico Geological Society, Guidebook 33, pp. 233–237.

Myers, D. A., and McKay, E. J., 1971, Geologic map of the Bosque Peak quadrangle, Valencia and Bernalillo Counties, New Mexico: U.S. Geological Survey, Geologic Quadrangle Map GQ-948, scale 1:24,000.

Myers, D. A., and McKay, E. J., 1972, Geologic map of the Capilla Peak quadrangle, Torrance and Valencia Counties, New Mexico: U.S. Geological Survey, Geologic Quadrangle Map GQ-1008, scale 1:24,000.

Myers, D. A., and McKay, E. J., 1974, Geologic map of the southwest quarter of the Torreon 15-minute quadrangle, Torrance and Valencia Counties, New Mexico: U.S. Geological Survey, Miscellaneous Investigations Map I-820, scale 1:24,000.

Myers, D. A., McKay, E. J., and Sharps, J. A., 1981, Geologic map of the Becker quadrangle, Valencia and Socorro Counties, New Mexico: U.S. Geological Survey, Geologic Quadrangle Map GQ-1556, scale 1:24,000.

Myers, D. A., Sharps, J. A., and McKay, E. J., 1986, Geologic map of the Becker SW and Cerro Montoso quadrangles, Socorro County, New Mexico: U.S. Geological Survey, Miscellaneous Investigations Map I-1567, scale 1:24,000.

Naeser, C. W., 1979, Fission-track dating and geologic annealing of fission tracks; *in* Jäger, E., and Hunziker, J. C. (eds.), Lectures in isotope geology: Springer–Verlag, New York, pp. 154–169.

New Mexico Bureau of Geology and Mineral REsurces, 2003, Geologic map of New Mexico, 1:5000,000: New Mexico Bureau of Geology and Mineral Resources.

Osburn, G. R., 1984, Geology of Socorro County: New Mexico Bureau of Mines and Mineral Resources, Open-file Report 238, 1 sheet, scale 1:200,000.

Peterson, J. A., 1980, Permian paleogeography and sedimentary provinces, west-central United States; *in* Fouch, T. D., and Magathan, E. R. (eds.), Paleozoic paleogeography of west-central United States: Society of Economic Paleontologists and Mineralogists, Rocky Mountain Section, Symposium 1, pp. 271–292.

Petit, J. P., 1987, Criteria for sense of movement on fault surfaces in brittle rocks: Journal of Structural Geology, v. 9, no. 5–6, pp. 509–608.

Pollock, C. J., Stewart, K. G., Hibbard, J. P., Wallace, L., and Giral, R. A., 2004 this volume, Structural geology of the west-central Sierra Nacimiento, New Mexico; *in* Cather, S. M., McIntosh, W. C., and Kelley, S. A. (eds.), Tectonics, geochronology, and volcanism in the southern Rocky Mountains and Rio Grande rift: New Mexico Bureau of Geology and Mineral Resources, Bulletin 160, pp. 97–112.

Rawling, G. C., and Goodwin, L. B., 2003, Cataclasis and particulate flow in faulted, poorly lithified sediments: Journal of Structural Geology, v. 25, no. 3, pp. 63–64.

Rehrig, W. A., and Heidrick, T. L., 1976, Regional tectonic stress during the Laramide and late Tertiary intrusive periods, Basin and Range province, Arizona: Arizona Geological Society, Digest, v. 10, pp. 205–228.

Reiche, P., 1949, Geology of the Manzanita and North Manzano Mountains, New Mexico: Geological Society of America, Bulletin, v. 60, no. 7, pp. 1183–1212.

Rodgers, J., 1987, Chains of basement uplifts within cratons marginal to orogenic belts: American Journal of Science, v. 287, no. 7, pp. 661–692.

Slack, P. B., and Campbell, J. A., 1976, Structural geology of the Rio Puerco fault zone and its relationship to central New Mexico tectonics; *in* Woodward, L. A., and Northrop, S. A. (eds.), Tectonics and mineral resources of southwestern North America: New Mexico Geological Society, Special Publication 6, pp. 46–52.

Smith, C. T., 1983, Structural problems along the east side of the Socorro constriction, Rio Grande rift; *in* Chapin, C. E., and Callender, J. F. (eds.), Socorro region II: New Mexico Geological Society, Guidebook 34, pp. 103–110.

Smith, C. T., Osburn, G. R., Chapin, C. E., Hawley, J. W., Osburn, J. C., Anderson, O. J., Rosen, S. D., Eggleston, T. L., and Cather, S. M., 1983, First day road log from Socorro to Mesa del Yeso, Joyita Hills, Johnson Hill, Cerros de Amado, Lomas de las Canas, Jornada del Muerto, Carthage, and return to Socorro; *in* Chapin, C. E., and Callender, J. F. (eds.), Socorro region II: New Mexico Geological Society, Guidebook 34, pp. 1–28.

Snyder, W. S., Dickinson, W. R., and Silberman, M. L., 1976, Tectonic implications of space-time patterns of Cenozoic volcanism in the western Unites States: Earth and Planetary Science Letters, v. 32, no. 1, pp. 91–106.

Stark, J. T., 1956, Geology of the South Manzano Mountains, New Mexico: New Mexico Bureau of Mines and Mineral Resources, Bulletin 34, 48 pp.

Stark, J. T., and Dapples, E. C., 1946, Geology of the Los Pinos Mountains, New Mexico: Geological Society of America, Bulletin, v. 57, no. 12, pp. 1121–1172.

Stewart, K. G., and Hibbard, J. P., 1992, Late Cretaceous thrust faulting at the eastern edge of the San Juan Basin, New Mexico; *in* Lucas, S. G., Kues, B. S., Williamson, T. E., and Hunt, A. P. (eds.), San Juan Basin IV: New Mexico Geological Society, Guidebook 43, pp. 7–9.

Stone, D. S., 1969, Wrench faulting and Rocky Mountain tectonics: The Mountain Geologist, v. 6, no. 2, pp. 67–79.

Tavarnelli, E., 1998, Tectonic evolution of the northern Salinian block, California, USA—Paleogene to Recent shortening in a transform fault-bounded continental fragment; *in* Holdsworth, R. E., Strachan, R. A., and Dewey, J. F. (eds.), Continental transpressional and transtensional tectonics: Geological Society, London, Special Publications 135, pp. 107–118.

Teyssier, C., Tikoff, B., and Markley, M., 1995, Oblique plate motion and continental tectonics: Geology, v. 23, no. 5, pp. 447–450.

Wilpolt, R. H., and Wanek, A. A., 1951, Geology of the region from Socorro and San Antonio east to Chupadera Mesa, Socorro County, New Mexico: U.S. Geological Survey, Oil and Gas Investigations Map OM-121, scale 1:62,500.

Wilson, J. E., 1999. Microfracture fabric of the Punchbowl fault zone, San Andreas system, California: Unpublished M.S. thesis, Texas A&M University, 125 pp.

Woodward, L. A., 1976, Laramide deformation of Rocky Mountain foreland—geometry and mechanics; *in* Woodward, L. A., and Northrop, S. A. (eds.), Tectonics and mineral resources of southwestern North America : New Mexico Geological Society, Special Publication 6, pp. 11–17.

Woodward, L. A., 2000, Implications of Jurassic, Cretaceous, and Proterozoic piercing lines for Laramide oblique-slip faulting in New Mexico and rotation of the Colorado Plateau—discussion: Geological Society of America, Bulletin, v. 112, no. 5, pp. 783–785.

Woodward, L. A., Anderson, O. J., and Lucas, S. G., 1997, Mesozoic stratigraphic constraints on Laramide right slip on the east side of the Colorado Plateau: Geology, v. 25, pp. 843–846.

Zoback, M. D., and Healy, J. H., 1992, In situ stress measurements to 3.5 km depth in the Cajon Pass scientific research borehole—implications for the mechanics of crustal faulting: Journal of Geophysical Research, v. 97, no. 4, pp. 5039–5057.

Zoback, M. D., Zoback, M. L ., Mount, V. S., Suppe, J., Eaton, J. P., Healy, J. H., Oppenheimer, D., Reasenberg, P., Jones, L., Raleigh, C. B., Wong, I. G., Scotti, O., and Wentworth, C., 1987, New evidence on the state of stress of the San Andreas fault system: Science, v. 238, pp. 1105–1111.